nature communications

Article

https://doi.org/10.1038/s41467-026-79754-5

ER-associated biogenesis of PINK1 preprotein for neuronal mitophagy

Received: 10 February 2026

Accepted: 28 October 2026

Published online: 20 November 2026

Check for updates

J. Tabitha Hees[1,7], Inmaculada Segura[1,7], Andrea Schneider[1], Martina Schifferer[2,3], Sultan Bekbayev[4], Jana Lindner[1], Simone Mattei[4,5], Thomas Misgeld[2,3,6] & Angelika B. Harbauer[1,3,6]

Given the large size of neurons, local maintenance of mitochondria is crucial to counteract insults to this organelle in axons and dendrites. The Parkinson-related mitochondrial kinase PINK1 plays a central role in mitochondrial quality control, which in neurons requires the transport of *Pink1* mRNA by mitochondrial hitch-hiking. However, how and where PINK1 is locally translated and processed has remained unclear. Using live-cell imaging, we trace local PINK1 translation sites and preprotein dynamics, revealing a concerted interplay between mitochondria and the ER, with endolysosomes frequently localized adjacent to the site of translation. Upon metabolically regulated untethering from mitochondria, *Pink1* mRNA relocates to ribosomes in proximity to the ER and endolysosomes for translation of the PINK1 preprotein. The ER chaperone DNAJB6 shields the PINK1 preprotein in transit to mitochondria, following the post-translational ER-SURF pathway. Consequently, loss of DNAJB6 leads to persistent ER/endolysosome-associated PINK1 precursor stores and failure of mitophagy upon mitochondrial damage. Our findings reveal that neuronal PINK1 protein translation switches between mitochondrially anchored co-translational and ER-associated post-translational import states, with functional implications for mitochondrial quality control.

Mitochondria are especially important in neurons, whose substantial energy demands are met largely by ATP generated through oxidative phosphorylation[1]. PTEN-induced kinase 1 (PINK1) senses mitochondrial damage and is crucial for neuronal health, as PINK1 mutations cause hereditary Parkinson's disease (PD)[2]. Like most nuclear-encoded mitochondrial precursors, PINK1 contains an N-terminal mitochondrial targeting sequence (MTS) followed by a transmembrane (TM) domain flanked by several regions important for its proper localization and processing (Fig. 1a, top)[3]. Unlike most MTS-containing proteins, PINK1 is incompletely imported because its TM domain is cleaved during import by the inner-membrane protease PARL. Cleaved PINK1 is then retro-translocated into the cytoplasm and degraded by the proteasome[4–7]. Upon mitochondrial damage, PINK1 remains unprocessed and stabilizes on the mitochondrial surface in close association with the translocase of the outer membrane (TOM complex)[8,9]. Stabilized PINK1 phosphorylates itself, several outer membrane proteins and ubiquitin[10–13], triggering Parkin recruitment and activation at mitochondria[14,15]. This initiates a signaling cascade that marks damaged mitochondria with phospho-ubiquitin chains[11,12,16]. These chains recruit autophagy adapters, including Optineurin, enabling selective autophagy of damaged mitochondria (mitophagy)[17,18].

[1]Max Planck Institute for Biological Intelligence, Martinsried, Germany. [2]German Center for Neurodegenerative Diseases, Munich, Germany. [3]Munich Cluster for Systems Neurology, Munich, Germany. [4]European Molecular Biology Laboratory, Molecular Systems Biology Unit, Heidelberg, Germany. [5]European Molecular Biology Laboratory, EMBL Imaging Centre, Heidelberg, Germany. [6]Technical University of Munich, School of Medicine and Health, Institute of Neuronal Cell Biology, Munich, Germany. [7]These authors contributed equally: J. Tabitha Hees, Inmaculada Segura. e-mail: angelika.harbauer@tum.de

https://doi.org/10.1038/s41467-026-79754-5

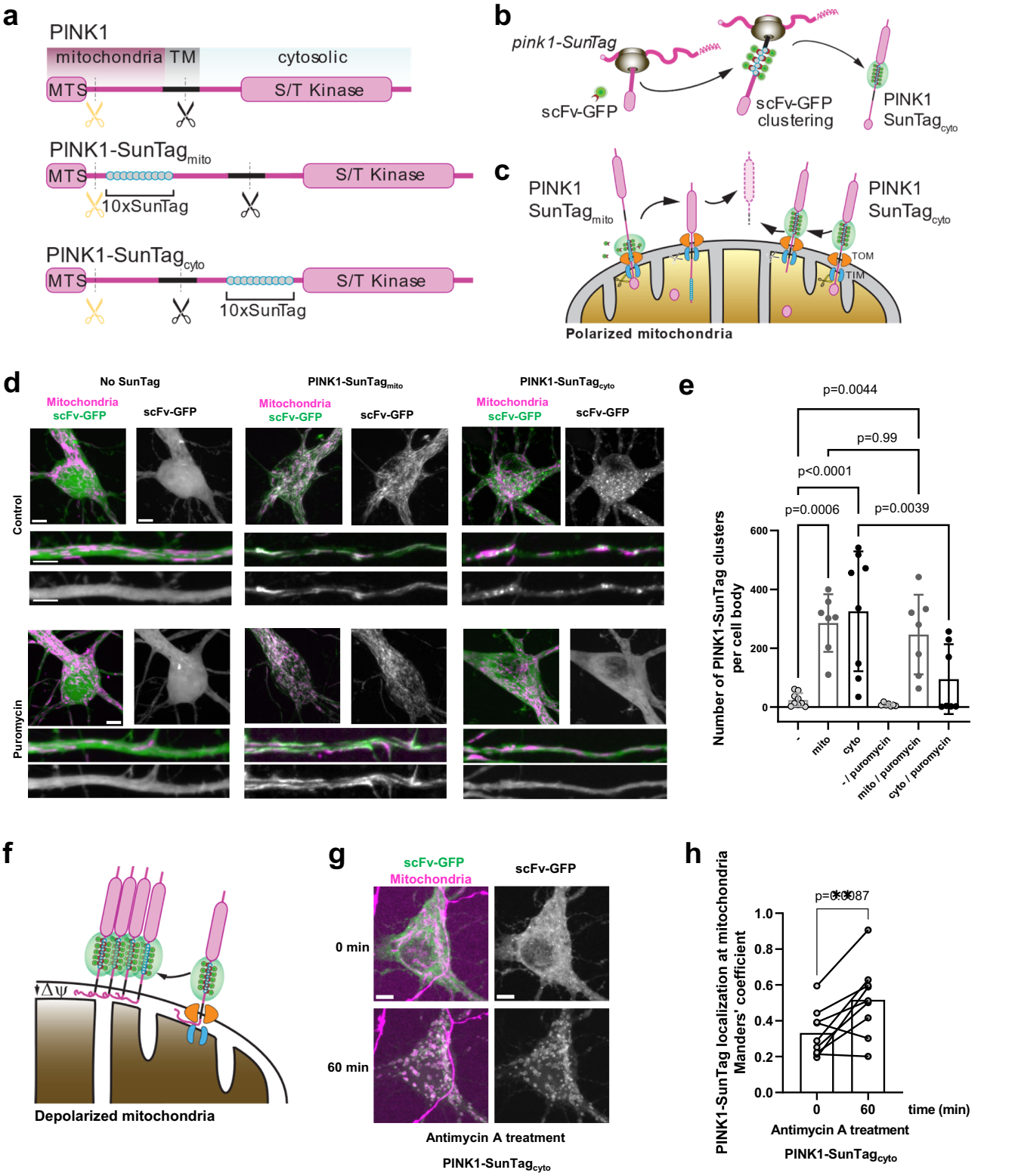

In neurons, transport of *Pink1* mRNA on the mitochondrial surface maintains a local supply of newly synthesized PINK1 precursor in axons and dendrites[19]. The RNA binding protein (RBP) Synaptojanin 2a (SYNJ2a) and its binding protein (SYNJ2BP) form an anchoring complex that tethers *Pink1* mRNA to mitochondria[19]. This association responds to cellular metabolism: insulin signaling suppresses it, while AMP-activated protein kinase (AMPK) activity enhances it by direct phosphorylation of SYNJ2BP[20]. Inhibiting insulin signaling or expressing a phospho-mimetic version of SYNJ2BP prevents mRNA release from mitochondria, lowering expression of PINK1 protein and restricting neuronal mitophagy[20]. Releasing *Pink1* mRNA from mitochondria increases the distance between translation and the protein's destination at mitochondria. This may delay import and thus alter the precursor's cytosolic transit route, potentially affecting PINK1 protein import and stabilization[21]. One possibility is a shift from co- to post-translational import, which was recently shown to be much more

Fig. 1 | A SunTag-based reporter that faithfully reports PINK1 processing in living cells. a Schematic representation of PINK1 protein domains and the PINK1-SunTag$_{mito}$ and PINK1-SunTag$_{cyto}$ reporters. A yellow scissor indicates MPP cleavage, a black scissor indicates a cleavage within the transmembrane segment by PARL. MTS mitochondrial targeting sequence, TM transmembrane domain, S/T Serine/Threonine. **b** Schematic depiction of the SunTag system adapted for the PINK1-SunTag preprotein reporter. **c** Comparison of the import and processing patterns expected upon insertion of the SunTag repeats within the PINK1 protein for PINK1-SunTag$_{mito}$ and PINK1-SunTag$_{cyto}$ reporters. Dashed lines indicate proteasomal degradation. TOM Translocase of the Outer Membrane, TIM Translocase of the Inner Membrane. **d** Representative images showing the distribution of either the scFv-GFP alone or cotransfected with either PINK1-SunTag$_{mito}$ or PINK1-SunTag$_{cyto}$ reporters (green) in somata and neurites of mouse hippocampal neurons. Mitochondria are visualized by coexpression of Cox8-BFP protein (magenta). Puromycin treatment was performed for 30 min at a concentration of 100 μg/ml. Black-white images correspond to the scFv-GFP signal only. **e** Quantification of images as in **d**. One-way ANOVA followed by Tukey's post hoc test; $n = 9–10$ (single cells coming from 2 independent biological replicates). **f** Schematic depiction of the accumulation of SunTag scFv-GFP on stabilized fully-synthesized PINK1-SunTag$_{cyto}$ upon mitochondrial depolarization. **g** Representative images showing the location of the PINK1-SunTag$_{cyto}$ reporter before and after incubation with 20 μM Antimycin A for 60 min. **h** Quantification of images as in (**g**). Paired two-sided Student's *t* test; $n = 9$ (single cells coming from 3 independent biological replicates). Data are expressed as mean ± SEM (**e**) or as mean (**h**). Scale bars, 5 μm for somas and neurites (**d, g**).

prevalent for mitochondrial proteins than previously appreciated[22,23]. Co-translational import limits the dwell time of the unfolded precursor in the cytoplasm, while post-translational import requires the interaction of mitochondrial precursors with chaperones to keep it unfolded until import. Some highly hydrophobic mitochondrial precursors have been described to peripherally associate with the endoplasmic reticulum (ER) and its chaperones during transit[24]. Because neuronal *Pink1* mRNA location changes with the metabolic state[20], we asked whether this induces a switch of import route and how this affects the ability of PINK1 to detect mitochondrial dysfunction.

To study the spatial distribution of the PINK1 preprotein in living neurons, we developed a SunTag-based reporter for the cytoplasmic location of the PINK1 preprotein[25]. This reporter faithfully recapitulates PINK1 processing and stabilization after mitochondrial damage. Releasing the mRNA from mitochondria produced larger and brighter SunTag clusters, consistent with a longer cytosolic transit of the PINK1 precursor. Intriguingly, the larger clusters not only colocalized with mitochondria, but also with endolysosomes and the ER, suggesting the ER contributes to PINK1 biogenesis. Also ribosomes were found near organellar assemblies of mitochondria, ER and endolysosomes in thin neurites. Large PINK1-SunTag clusters colocalized with the chaperone DNAJB6, consistent with usage of the post-translational ER-surface retrieval pathway (ER-SURF) whenever PINK1 is translated near the ER[24]. DNAJB6 knockdown impaired PINK1-dependent mitophagy, despite ongoing PINK1 protein synthesis, indicating that this chaperone supports transfer of the PINK1 precursor to mitochondria. Together, our findings reveal that neuronal PINK1 import switches between mitochondrially anchored co-translational import and ER-associated post-translational retrieval, with mitochondria, ER and endolysosomes cooperating for local mitochondrial quality control.

Results

A live-cell reporter that faithfully reports PINK1 processing

The SunTag system uses an intracellular single chain variable fragment antibody fused to superfolder GFP (mouse scFv-GFP) recognizing a short epitope derived from yeast GCN4 inserted repetitively in frame into a protein of interest[25]. As the nascent chain emerges from the ribosome, scFv-GFP clusters on the SunTag epitopes (Fig. 1b). As import into mitochondria only allows unfolded protein entry, this reporter will accompany PINK1 whenever it resides in the cytosol. We created plasmids expressing kinase-dead PINK1 with 10 SunTag repeats inserted either between the MTS and the TM (PINK1-SunTag$_{mito}$) or just before the cytosolic kinase domain (PINK1-SunTag$_{cyto}$, Fig. 1a) to compare their effect on PINK1 location and processing. PINK1-SunTag$_{mito}$ import would place the entire SunTag repeats within mitochondria and thus import terminates the signal as the TOM complex only admits unfolded proteins. PINK1-SunTag$_{cyto}$ would not require the internalization of the epitopes before the PINK1 TM is processed by PARL[4]. The signal will be terminated by degradation of the cleaved PINK1-SunTag$_{cyto}$ (Fig. 1c).

In cultured primary hippocampal neurons, both reporters produced bright GFP signals near mitochondria, unlike scFv-GFP alone (Fig. 1d). PINK1-SunTag$_{mito}$ outlined mitochondria, whereas PINK1-SunTag$_{cyto}$ formed small round clusters throughout the soma and processes (Fig. 1d, upper panels). Importantly, the PINK1-SunTag$_{cyto}$ signal was sensitive to translational inhibition induced by puromycin (100 μg/ml, 30 min; Fig. 1d, e), supporting that these small clusters indeed represented newly synthesized PINK1, unlike the PINK1-SunTag$_{mito}$ signal (Fig. 1d). This difference was observed in both somatic and dendritic areas (Fig. 1d).

To determine, which reporter represents the known kinetics of PINK1 import best, we analyzed the cleavage of PINK1-SunTag$_{cyto}$ and PINK1-SunTag$_{mito}$, the ability of the reporter constructs to accumulate on depolarized mitochondria, and the stabilization of the cleaved product by proteasomal inhibition. Endogenous PINK1 preprotein is first cleaved after its MTS by the matrix metalloprotease MPP and afterwards within its TM by PARL[4,5]. Treatment with mitochondrial uncouplers such as CCCP stabilizes full length PINK1, whereas the processed form is stabilized by the proteasome inhibitor MG-132[4,26]. Due to its incomplete import, PINK1 is accessible to treatment with proteinase K (PK) on isolated mitochondria. PINK1-SunTag$_{cyto}$ reproduced these properties: the respective forms could be stabilized by CCCP (100 μM, 2 h) and MG-132 (10 μM, 2 h), and it remained PK accessible (Supplementary Fig. 1a). By contrast, PINK1-SunTag$_{mito}$ accumulated an alternative intermediate (Supplementary Fig. 1b), most likely processed by MPP but not PARL[5]. The earlier insertion thus interferes with the processing of the reporter, explaining its persistent mitochondrial surface signal, as PARL cleavage is necessary for timely PINK1 degradation[4]. This non-physiological intermediate also fails to stabilize upon either MG-132 or CCCP treatment and remains inaccessible to PK (Supplementary Fig. 1b). Impaired processing was observed regardless of scFv-GFP expression (Supplementary Fig. 1c, d). Thus, PINK1-SunTag$_{cyto}$ best represents the newly synthesized preprotein until its partial import into healthy mitochondria, its processing and proteasomal degradation.

Additionally, PINK1-SunTag$_{cyto}$ should reflect mature PINK1 after stabilization on depolarized mitochondria (Fig. 1f). Indeed, upon treatment of primary neurons with the complex III inhibitor Antimycin A (AA; 20 μM, 1 h), PINK1-SunTag$_{cyto}$ formed rings surrounding mitochondria (Fig. 1g, h). This aligns with PINK1 accumulation at the surface of depolarized mitochondria and is clearly distinct from the small clusters observed near polarized mitochondria (Fig. 1d, g). We therefore chose the PINK1-SunTag$_{cyto}$ reporter for our following experiments (from now on referred to as PINK1-SunTag).

Cytosolic PINK1 clusters upon *Pink1* mRNA release from mitochondria

Under basal conditions, PINK1-SunTag localized near mitochondria, consistent with the mitochondrial association of the *Pink1* mRNA[19]. Inhibition of AMPK signaling using either the inhibitor Compound C (CC) or insulin stimulation releases the mRNA from its mitochondrial

https://doi.org/10.1038/s41467-026-79754-5

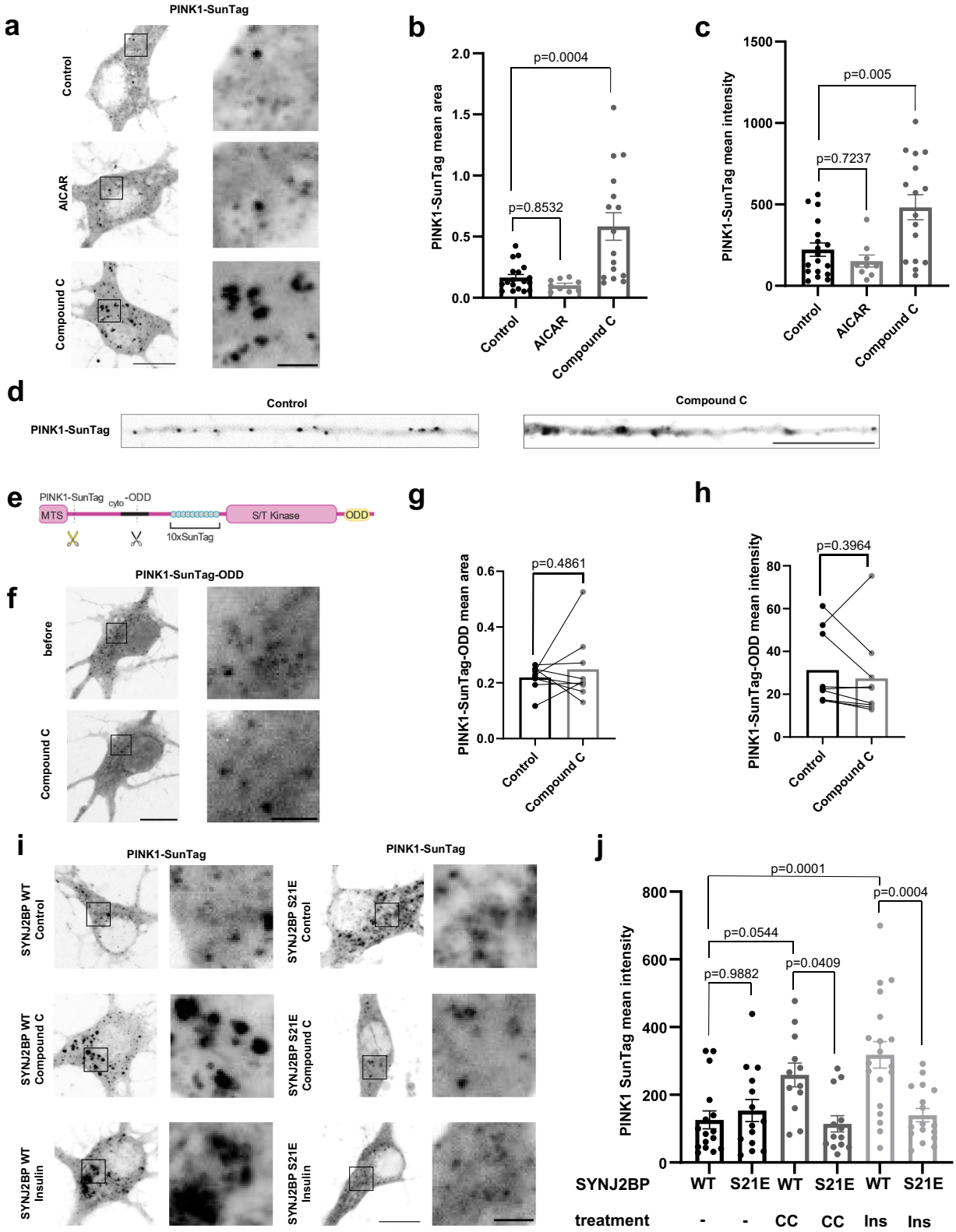

tether, without increasing its abundance[20]. Both treatments (CC 20 μM, 2 h; insulin 500 nM, 1 h) increased PINK1-SunTag clusters in size and intensity in somata and dendrites (Fig. 2a–d and Supplementary Fig. 2a–c), consistent with our previous observation of increased endogenous PINK1 levels in human iPSC-derived cortical neurons in the presence of insulin signaling[20]. The AMPK activator AICAR (1 mM, 2 h) did not significantly alter either PINK1-SunTag cluster size or intensity (Fig. 2a–c), as AMPK activity is already high in the insulin-free imaging medium. The effect of insulin on PINK1-SunTag clusters was blocked by pre-treatment with Wortmannin (1 μM, 2 h), an inhibitor of the phosphatidylinositol 3-kinase acting downstream of the insulin signaling (Supplementary Fig. 2a–c). Importantly, neither insulin-deficient media (Hibernate E for 2 h) nor addition of CC for 2 h altered overall translation in neurons measured by puromycin incorporation (Supplementary

Fig. 2 | Cytosolic PINK1-SunTag clusters upon *Pink1* mRNA release from mitochondria. a Representative images of cytosolic PINK1 protein clusters visualized by the SunTag system upon either control conditions or AMPK activation or inhibition using AICAR (1 mM, 2 h) or CC (20 μM, 2 h), respectively, in mouse hippocampal neurons. Magnified insets of the indicated regions are shown to the right. **b** Quantification of the PINK1 protein cluster mean area as in **a** (data points represent the average cluster area across all clusters within an individual neuron). One-way ANOVA followed by Tukey's post hoc test; $n = 9–18$ (single cells coming from 3 independent biological replicates). **c** Quantification of the PINK1 protein cluster mean intensity as in (**a**) (data points represent the average cluster intensity across all clusters within an individual neuron, background-subtracted). One-way ANOVA followed by Tukey's post hoc test; $n = 9–18$ (single cells coming from 3 independent biological replicates). **d** Representative images of cytosolic PINK1 protein clusters visualized by the SunTag system upon control (untreated) or CC (20 μM, 2 h) treatment in neurites of hippocampal neurons. **e** Schematic representation of the PINK1-SunTag$_{mito}$-ODD reporter. A yellow scissor indicates MPP cleavage, a black scissor indicates a cleavage within the transmembrane segment by PARL. MTS mitochondrial targeting sequence, TM transmembrane domain, S/T Serine/Threonine, ODD Oxygen degradation domain. **f** Representative images of cytosolic PINK1-SunTag$_{mito}$-ODD protein clusters visualized by the SunTag system before and after CC (20 μM, 2 h) treatment in mouse hippocampal neurons. Magnified insets of the indicated regions are shown to the right. **g** Quantification of the PINK1 protein cluster mean area as in (**f**) (data points represent the average cluster area across all clusters within an individual neuron). Paired two-sided Student's *t* test; $n = 9$ (single cells coming from 2 independent biological replicates). **h** Quantification of the PINK1 protein cluster mean intensity as in (**f**) (data points represent the average cluster intensity across all clusters within an individual neuron, background-subtracted). Paired two-sided Student's *t* test; $n = 9$ (single cells coming from 2 independent biological replicates). **i** Representative images of cytosolic PINK1 protein clusters visualized by the SunTag system in hippocampal neurons overexpressing either SYNJ2BP WT or S21E and treated with either control (untreated), CC (20 μM, 2 h) or insulin (ins, 500 nM, 1 h). Magnified insets of the indicated regions are shown to the right. **j** Quantification of the PINK1 protein cluster mean intensity as in (**i**) (data points represent the average cluster intensity across all clusters within an individual neuron, background-subtracted). One-way ANOVA followed by Tukey's post hoc test; $n = 12–19$ (single cells coming from 3 independent biological replicates). Data are expressed as mean ± SEM (**b, c, j**) or mean (**g, h**). Scale bars, 10 μm for whole soma and neurite, 2 μm for insets.

Fig. 2d, e). CC also did not cause unspecific clustering of the scFv-GFP without the PINK1-SunTag reporter (Supplementary Fig. 2f), nor did it alter processing of the PINK1-SunTag construct (Supplementary Fig. 2g). To test whether this increased signal represents an accumulation of fully synthesized PINK1 precursor in transit to mitochondria, we added an oxygen-dependent degradation domain (ODD)[27,28] to the C-terminus of the PINK1-SunTag$_{cyto}$ reporter (Fig. 2e). After synthesis, oxygen-dependent prolyl hydroxylase domain proteins target ODD-tagged proteins for degradation, without requiring mitochondrial protein import. CC or insulin-treatment no longer elicited increased cluster areas if PINK1-SunTag$_{cyto}$-ODD was used (Fig. 2f, g and Supplementary Fig. 2h, i), supporting the conclusion that the increase in PINK1-SunTag signal represents a cytosolic pool of fully synthesized PINK1 in transit to the mitochondrial import pore. Directly targeting the PINK1-SunTag$_{cyto}$ reporter to the proteasome also prevented the observed increase in intensity (Fig. 2h and Supplementary Fig. 2j), suggesting that the increased abundance of PINK1 protein observed upon CC or insulin treatment is not due to a change in the number of ribosomes engaged in translation, but due to a cytosolic accumulation of the preprotein.

A phosphomimetic SYNJ2BP mutant (S21E) retains *Pink1* mRNA at mitochondria despite AMPK inhibition[20]. Overexpressed SYNJ2BP-S21E prevented the increased intensity of PINK1-SunTag clusters upon CC or insulin treatment in mouse hippocampal neurons, unlike wild-type (WT) SYNJ2BP (Fig. 2i, j). Neither the size nor the intensity of PINK1-SunTag clusters significantly changed upon AMPK inhibition in HeLa cells (Supplementary Fig. 2k–m), consistent with the requirement for the neuronally enriched RBP SYNJ2a for *Pink1* mRNA anchoring[19]. Thus, *Pink1* mRNA localization governs the formation of larger PINK1-SunTag clusters in neuronal somata and neurites, likely reflecting precursor in transit.

PINK1-SunTag clusters contain translating ribosomes

To test whether the PINK1-SunTag clusters represent a physiological pool of newly synthesized PINK1, we tested whether translating ribosomes are necessary for the formation and present within these clusters.

Simultaneous addition of the translation inhibitor puromycin and CC prevented the formation of large PINK1-SunTag clusters, indicating that their formation requires ongoing synthesis and does not result from preprotein aggregation (Fig. 3a–c). To assess endogenous PINK1 turnover in insulin-containing media, we took advantage of an anti-human PINK1-specific antibody and treated human iPSC-derived cortical neurons with the translation inhibitor cycloheximide (CHX) (Supplementary Fig. 3a, b). Despite a three-fold increase in PINK1 protein under insulin-mediated AMPK inhibition, the levels returned to baseline 30 min after CHX addition, indicating unaltered turnover of PINK1 (Supplementary Fig. 3a, b).

We also tracked *Pink1* mRNA and PINK1 precursors simultaneously by combining SunTag imaging with the MS2/PP7 split-Venus imaging system by incorporation of MS2/PP7 RNA loops into the 3′ untranslated region of the PINK1-SunTag reporter[19,20,29]. Split-Venus tagged MS2 and PP7 coat allowed the detection of the mRNA, while the preprotein was detected with red fluorescent tagged scFv (Fig. 3d). Upon CC treatment, much of the PINK1-SunTag cluster area overlapped with *Pink1* mRNA, though some mRNA and preprotein signals did not overlap (Supplementary Fig. 3c). Together with the puromycin sensitivity of the PINK1-SunTag clusters, this suggests that many PINK1-SunTag clusters include ongoing translation events in addition to fully synthesized PINK1 preprotein in transit. The lower abundance of mRNA in neurites allowed us to resolve the spatial coordination between *Pink1* mRNA, PINK1-SunTag, and mitochondria upon insulin-induced AMPK inhibition in more detail. Under control conditions, mRNA and SunTag signal overlapped near mitochondria in both axons and dendrites (Fig. 3e, f, upper panels, white arrowheads). Insulin increased their distance from mitochondria in several cases (Fig. 3e, f, lower panels, yellow arrowheads). Interestingly, the localization of several *Pink1* mRNA dots remained fixed within the neurite, while mitochondrial movement led to the observed decrease in proximity (Fig. 3e, f). In some instances, SunTag signal bridged the gap between mRNA and mitochondria (Fig. 3e, f, lower panels, yellow asterisk), consistent with precursor moving from its synthesis site (marked by the mRNA as a proxy for the location of the ribosome) toward mitochondrial import pores.

Using a proximity ligation assay (PLA) between an antibody recognizing the ribosomal protein Rps6 and an antibody recognizing scFv-GFP, we tested whether ribosomes are indeed present in the CC-induced PINK1-SunTag clusters, as this assay will only yield a fluorescent signal if the two proteins are less than 40 nm apart[19,30] (Supplementary Fig. 3d). PLA signal almost ubiquitously colocalized with large PINK1-SunTag clusters upon CC treatment (Supplementary Fig. 3e), but was absent if scFv-GFP alone was used (Supplementary Fig. 3e) or if anti-Rps6 antibody was omitted (Supplementary Fig. 3f). CC also did not substantially alter Rps6 distribution (Supplementary Fig. 3g).

Finally, we utilized PLA after puromycylation (Puro-PLA) to assay endogenous PINK1 translation in human iPSC-derived cortical neurons[31]. A short low concentration pulse of puromycin (10 μg/ml, 5 min) leads to puromycin incorporation into nascent

https://doi.org/10.1038/s41467-026-79754-5

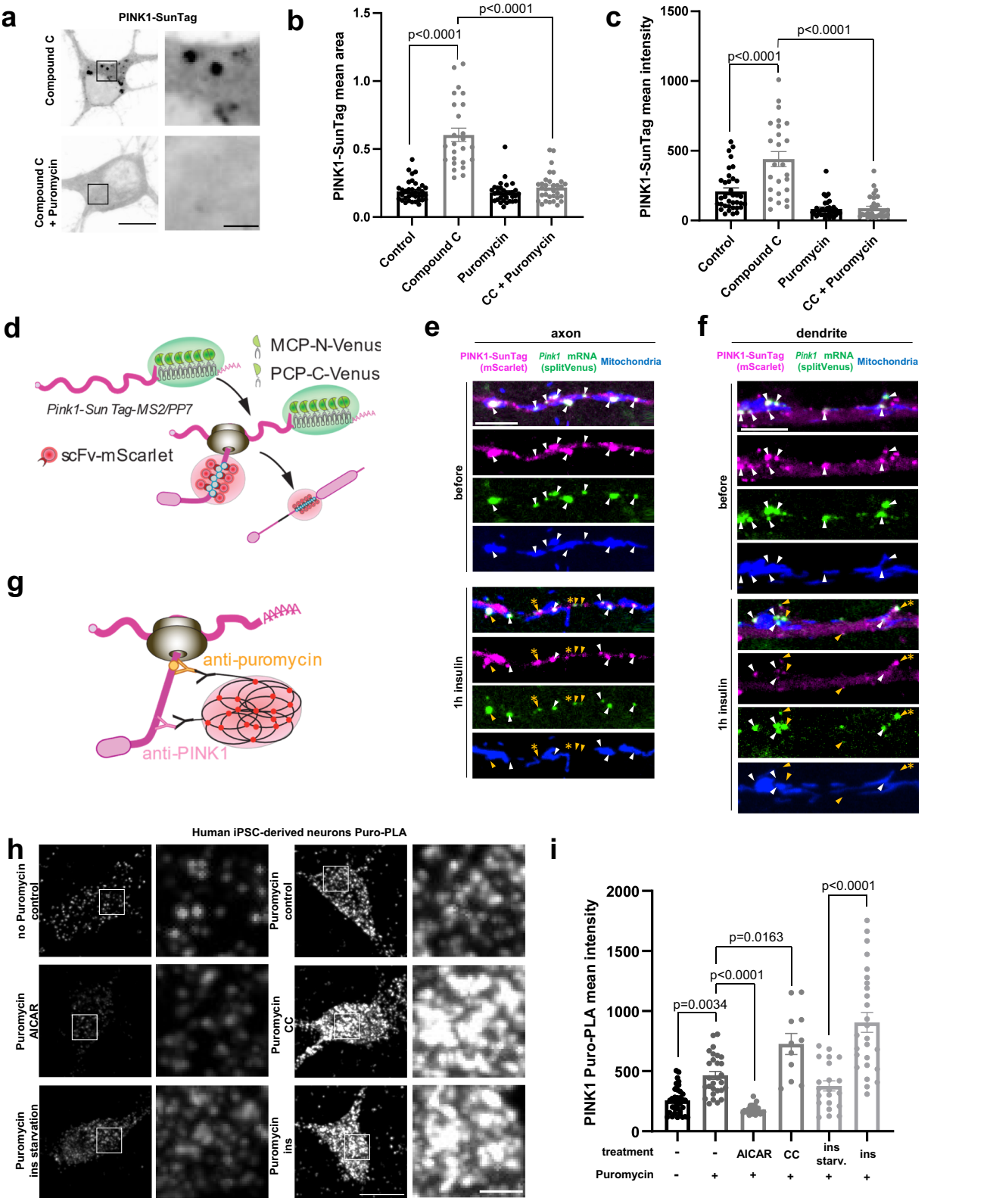

chains rather than global translational inhibition. The Puro-PLA signal (using anti-PINK1 and anti-puromycin antibodies, Fig. 3g) confirmed an increased presence of newly translated PINK1 upon CC or insulin addition (Fig. 3h, i). In contrast, activation of AMPK by either AICAR treatment (1 mM) or insulin withdrawal for 2 h reduced PLA intensity to background levels (Fig. 3h, i). Together, these observations indicate that the larger PINK1-SunTag clusters represent a physiological pool of newly synthesized, cytoplasmic PINK1.

Cytosolic PINK1 clusters near endolysosomes provide PINK1 protein to mitochondria

Because AMPK inhibition reduces mitochondrial mRNA association and induces cytosolic PINK1-SunTag clusters, we tested their

Fig. 3 | PINK1-SunTag clusters contain translating ribosomes. a Representative images of cytosolic PINK1 protein clusters visualized by the SunTag system upon CC (20 μM, 2 h) or simultaneous treatment with CC and puromycin (200 μg/ml, 2 h) in hippocampal neurons. Magnified insets of the indicated regions are shown to the right. **b** Quantification of the PINK1 protein cluster mean area following puromycin and CC treatments as in (**a**) (data points represent the average cluster area across all clusters within an individual neuron). One-way ANOVA followed by Tukey's post hoc test; $n = 25–35$ (single cells coming from 6 independent biological replicates). **c** Quantification of the PINK1 protein cluster mean intensity following Puromycin and CC treatments as in (**a**) (data points represent the average cluster intensity across all clusters within an individual neuron, background-subtracted). One-way ANOVA followed by Tukey's post hoc test; $n = 25–35$ (single cells coming from 6 independent biological replicates). **d** Schematic of dual *Pink1* mRNA and protein visualization using MS2/PP7 and SunTag. Signals indicate three functional states: *Pink1* mRNA (Venus only), active translation of *Pink1* mRNA (Venus and mScarlet), and released PINK1 preprotein (mScarlet only). Representative images of an axon (**e**) and dendrite (**f**) of hippocampal neurons expressing the dual-labeling reporter (PINK1 SunTag using scFv-mScarlet in magenta; *Pink1* mRNA using reconstituted splitVenus in green) as depicted in (**d**), together with BFP-labeled mitochondria (blue), before and after insulin (100 μg/ml, 1 h) treatment. White arrowheads mark *Pink1* mRNA in close proximity to mitochondria, whereas yellow arrowheads showcase mRNA without direct mitochondrial association. The same straightened neurites before and after treatment are shown. Instances where the PINK1-SunTag signal bridges the location of the Venus-labeled mRNA with the nearest mitochondrion are marked with a yellow asterisk. Please note that several Venus positive dots remain in the same relative location, whereas mitochondrial movement creates the observed increase in distance. **g** Schematic illustrating the proximity ligation assay coupled with puromycylation (Puro-PLA) for PINK1. **h** Representative images of PINK1-Puro-PLA signal in human iPSC-derived neurons either untreated (control) or treated with AICAR (1 mM, 2 h), CC (20 μM, 2 h), insulin (500 nM, 1 h) or in insulin-free medium (ins. starvation, 2 h), combined with or without puromycin treatment as indicated (10 μg/ml, 5 min). Magnified insets of the indicated regions are shown to the right. **i** Quantification of the mean intensity of the PINK1-Puro PLA signal as in (**h**). One-way ANOVA followed by Tukey's post hoc test; $n = 11–39$ (single cells coming from 2 independent biological replicates). Data are expressed as mean ± SEM. Scale bars, 10 μm for whole soma (**a, h**), 2 μm for insets (**a, h**), 5 μm for axon/dendrite (**e, f**).

relationship to other organelles. Rab7-positive late endosomes/endolysosomes serve as translational hotspots for nuclear-encoded mitochondrial transcripts in neurons[32]. In control conditions, PINK1-SunTag colocalized more with mitochondria than with Rab7-positive late endosomes (Fig. 4a, b), but CC treatment induced a significant shift towards Rab7-positive late endosomes (Fig. 4a, b). Under control conditions, PINK1-SunTag also barely colocalized with TMEM192-positive endolysosomes or Lamp1-positive lysosomes, which interconvert from endosomes[33]. CC treatment induced an even stronger redistribution of PINK1-SunTag towards these more mature endolysosomal vesicles (Fig. 4a, b), although some mitochondrial colocalization remained (Fig. 4a–c). Rotation of channels by 90 degrees before determining the Manders' coefficient to simulate a random cytosolic distribution eliminated the CC effect, arguing that the observed changes in organellar localization were not caused by the altered size or number of SunTag clusters (Supplementary Fig. 4a–d). Furthermore, this shift in localization was mirrored by the distribution of *Pink1* mRNA towards endolysosomes following CC treatment (Supplementary Fig. 4e, f)[20]. Importantly, overexpression of SYNJ2BP-S21E, which maintains *Pink1* mRNA association with mitochondria, prevented the CC- and insulin-induced redistribution of PINK1-SunTag (Supplementary Fig. 4g–i), while simultaneously reducing PINK1-SunTag cluster intensity (see Fig. 2i, j, analyzing the same set of neurons).

The observed remaining association of the PINK1-SunTag reporter with mitochondria and its induced colocalization with endolysosomes upon CC treatment, together with the presence of ribosomes, suggested that PINK1 translation occurs at mitochondria-endolysosomal contact sites. We therefore tested whether PINK1-SunTag clusters colocalized with both organelles in somata and neurites of mouse hippocampal neurons in culture. Under control conditions, neurons showed low triple colocalization, but CC treatment increased the amount of PINK1-SunTag contacting both organelles (Fig. 4d, e).

To visualize the journey of the PINK1 protein from its site of synthesis towards depolarized mitochondria, we performed live-cell imaging of neurons pre-treated with insulin (500 nM, 1 h) to enhance PINK1 synthesis, followed by AA treatment (20 μM) to induce mitochondrial damage. We observed that the PINK1-SunTag signal located at mitochondria-endolysosomal contact sites after insulin treatment moved away from endolysosomes and towards mitochondria following AA treatment (Fig. 4f left, Supplementary Video 1), sometimes in concert with mitochondrial shrinkage, typical of mitochondrial damage (Fig. 4f right, Supplementary Video 2). Damaged mitochondria appeared surrounded by a halo of stabilized PINK1 as previously observed (Fig. 1f–h). This confirms that the cytoplasmic pool of PINK1 is used to demarcate damaged mitochondria.

ER tubules contribute to PINK1 biogenesis

To resolve membranes of mitochondria and endolysosomes near the cytoplasmic stores of newly synthesized PINK1, we performed correlative light and electron microscopy (CLEM) in CC-treated neurons (Fig. 5a, b). Large PINK1-SunTag clusters were indeed in close apposition to endolysosomes and mitochondria (Fig. 5a, b). Surprisingly, we identified ER tubules overlapping the PINK1-SunTag signal in-between mitochondria and endolysosomes (Fig. 5b inset, green arrowheads), suggesting that the ER might bridge both organelles and contribute to PINK1 translation.

To further validate the architecture of these contact sites inside the neurites of CC-treated neurons, we performed cryo-electron tomography (cryo-ET), focusing on thin neurites positive for Lysotracker as a marker for endolysosomes. Tomographic reconstruction revealed that ER tubules were frequently weaving through the gaps between mitochondria and endolysosomes (Supplementary Video 3). This arrangement appeared in approximately 50% of all tomograms containing all three organelles (59 out of 122 tomograms). Subtomogram averaging identified ribosomes at a resolution of 22 Å and mapped them in the tomogram (Fig. 5c). Only few ribosomes were identified in each tomogram, as expected in axons (5–20 ribosomes/tomogram). Importantly, while many ribosomes were in proximity to the mitochondria or ER (Supplementary Fig. 5a), their random orientation suggests they were not targeted to membranes through translation of secretory proteins (Supplementary Fig. 5b).

To test whether endogenous *Pink1* mRNA indeed associates with ribosomes at these locations, we performed proximity biotinylation of ribosomes bearing AviTagged-Rpl10a near organellar membranes (Fig. 5d)[34]. The Avi-specific BirA Ligase was co-expressed in primary cortical mouse neurons as a cytosolic, an ER-targeted (Sec61β-BirA), a mitochondrial outer membrane-targeted (Fis1-BirA), or a Rab7-targeted (Rab7-BirA) protein. Upon CC treatment, the amount of *Pink1* mRNA associated increased with organelle-associated biotinylated ribosomes, while the fraction in cytoplasmic ribosomes was slightly reduced (Fig. 5e). A control transcript (*actin*) remained unresponsive to AMPK inhibition (Supplementary Fig. 5c, d). Thus, membrane-associated ribosomes at ER–endolysosome–mitochondria contacts are a major source of PINK1 precursor after mRNA release from mitochondria.

As SYNJ2BP can interact with the ribosome binding protein 1 (RRBP1), an ER-localized protein that forms a contact site rich in ribosomes[35,36], we tested RRBP1's role in PINK1 translation. PLA

https://doi.org/10.1038/s41467-026-79754-5

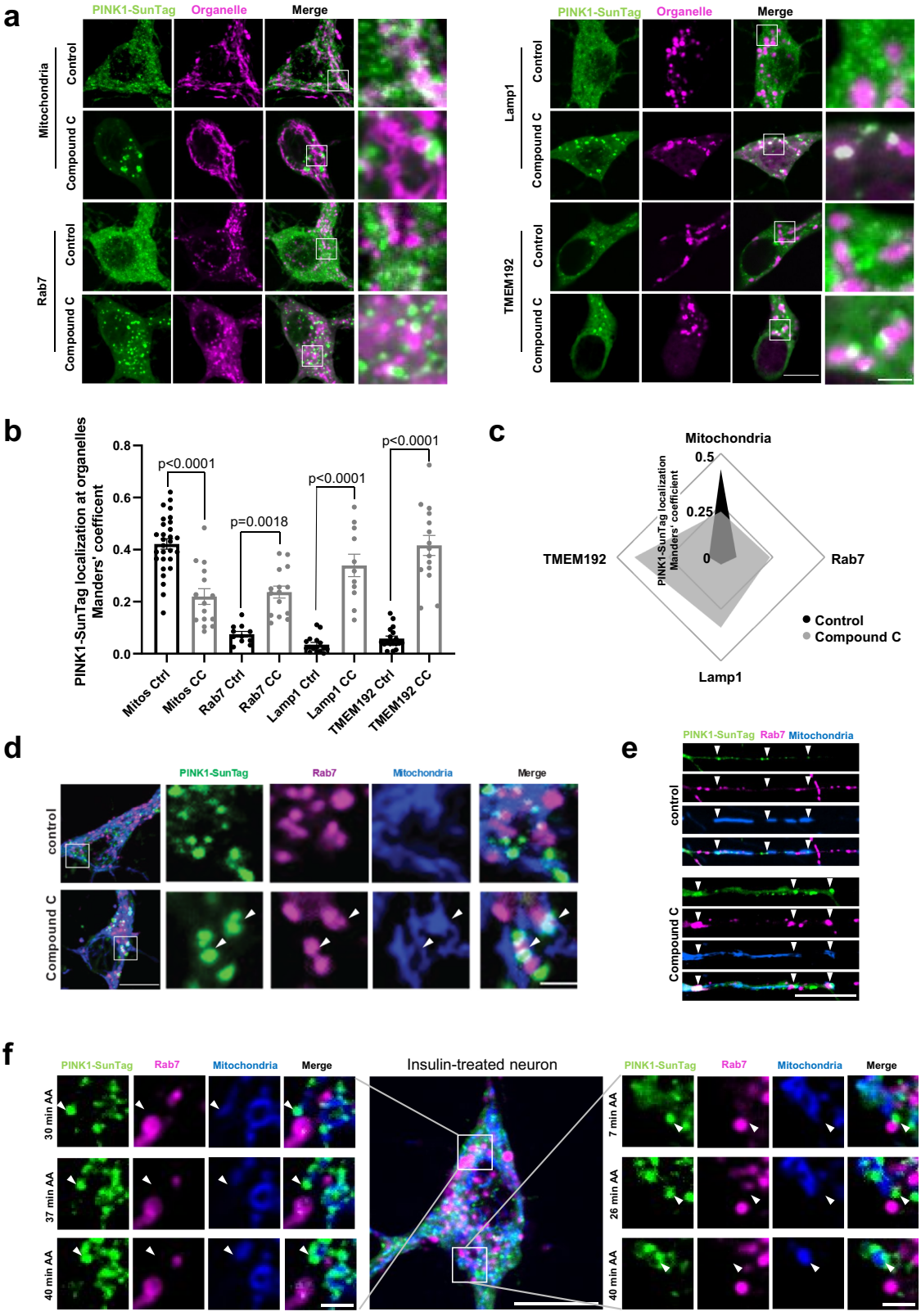

experiments revealed that CC treatment specifically enhanced the proximity between RRBP1 and the PINK1-SunTag reporter (Fig. 5f, g), but no difference was observed when Sec61β (another ribosomal receptor on the ER) was analyzed (Supplementary Fig. 5e, f). However, silencing of RRBP1 by shRNA (Supplementary Fig. 6a, b) did not alter the localization of the large CC-induced PINK1-SunTag clusters (Supplementary Fig. 6c–e). To test whether RRBP1 was required for PINK1 activity at mitochondria, we assayed the PINK1-dependent phosphorylation of ubiquitin in response to mitochondrial damage. Silencing of RRBP1 did not prevent PINK1 activity at mitochondria

Fig. 4 | Cytosolic PINK1 clusters are localized at endolysosomes upon AMPK inhibition. a Representative images of cytosolic PINK1 protein clusters visualized by the SunTag system and fluorescently-labeled organelles (Cox8-mRaspberry (mitochondria), Rab7A-mCherry (endosomes), LAMP1-mCherry (lysosomes) or TMEM192-RFP (endolysosomes)) upon control (untreated) or CC (20 μM, 2 h) treatment in hippocampal neurons. Magnified insets of the indicated regions are shown to the right. **b** Quantification of the Manders' coefficient of the colocalization between the PINK1-SunTag signal and the respective organellar signal as in (**a**). One-way ANOVA followed by Tukey's post hoc test; $n = 11–29$ (single cells coming from 3 independent biological replicates). **c** Radar chart illustrating PINK1-SunTag organelle colocalization as in (**b**). The four corners represent the tested organelles (mitochondria, Rab7-, LAMP1-, and TMEM192-positive endolysosomes). The distance from the center to the corners indicates the respective Manders' coefficient, either in control (untreated) cells (black) or upon CC (20 μM, 2 h) treatment (gray). Please note that treatment induces a shift in colocalization towards endolysosomes, while retaining partial mitochondrial localization. **d** Representative images and magnified insets of cytosolic PINK1 protein clusters visualized by the SunTag system and fluorescently-labeled organelles (mito-BFP and Rab7-mCherry) upon control (untreated) or CC (20 μM, 2 h) treatment in the soma of hippocampal neurons. Arrowheads point to regions where PINK1 SunTag clusters, late endosomes and mitochondria are in close proximity. **e** Representative images of cytosolic PINK1 protein clusters visualized by the SunTag system and fluorescently-labeled organelles (mito-BFP and Rab7-mCherry) upon control (untreated) or CC (20 μM, 2 h) treatment in a neurite of hippocampal neurons. Arrowheads point to PINK1 SunTag clusters at mitochondria without (control) or with (CC) a late endosome in proximity. **f** Representative image and magnified insets of cytosolic PINK1 protein clusters visualized by the SunTag system and fluorescently-labeled organelles (mito-BFP and Rab7-mCherry) in an insulin (500 nM, 1 h)-treated hippocampal neuron followed by 20 μM AA treatment. Arrowheads point to PINK1 SunTag clusters at mitochondria-late endosome contact sites moving away from the endolysosome and towards mitochondria. Data are expressed as mean ± SEM (**b**) or mean (**c**). Scale bars, 10 μm for whole soma and neurite, 2 μm for insets.

(Supplementary Fig. 6f, g). RRBP1 is therefore associated with ER-localized PINK1 clusters but is not essential for translation or preprotein transfer to mitochondria.

PINK1 requires DNAJB6 to exit the ER-associated clusters

In yeast, ER-associated chaperones such as Djp1 guide mitochondrial precursors to mitochondria through the ER-SURF pathway[24,37]. We therefore tested whether the chaperone DNAJB6, the mammalian homolog of Djp1, colocalized with the PINK1-SunTag clusters induced by CC treatment. Indeed, DNAJB6 colocalized clearly in clusters together with the PINK1-SunTag reporter upon CC treatment (Fig. 6a). Importantly, we observed similar clustering of endogenous DNAJB6 upon CC treatment in non-transfected neurons (Fig. 6b, c), showing that this effect was independent of PINK1 overexpression. Knockdown of PINK1 by a previously validated shRNA[38] did not prevent the clustering of DNAJB6 in response to CC treatment, suggesting that either other substrates or residual PINK1 are sufficient for the formation of DNAJB6 clusters in response to CC (Supplementary Fig. 7a, b). DNAJB6 clustering was not observed in HeLa cells (Supplementary Fig. 7c), suggesting that it is a neuron-specific phenomenon. DNAJB6 knock down (Supplementary Fig. 7d, e)[39] did not prevent the formation or change the localization of the large PINK1-SunTag clusters in neurons in response to CC (Supplementary Fig. 7f–h), consistent with a role of the chaperone downstream of PINK1 translation.

To test whether DNAJB6 enables transfer of PINK1 from ER-associated stores to damaged mitochondria, we analyzed by PLA the association of PINK1-SunTag clusters with RRBP1, as before. In CC-treated neurons, mitochondrial depolarization using AA significantly reduced the PLA signal, indicating that PINK1 relocates away from ER-localized RRBP1. However, in the absence of DNAJB6, PINK1-SunTag remained close to the ER-localized RRBP1 (Fig. 6d, e), suggesting that DNAJB6 is required for efficient transfer to depolarized mitochondria.

Loss of DNAJB6 impairs PINK1-dependent mitophagy

Thus, we examined whether DNAJB6 deficiency prevented the precursor from reaching mitochondria to execute its function in mitophagy. In control neurons, induction of mitochondrial damage by AA triggered a clear redistribution of PINK1-SunTag clusters away from endolysosomes and towards mitochondria, consistent with successful precursor transfer. In contrast, DNAJB6 silencing prevented the recruitment and stabilization of PINK1 in response to mitochondrial damage after AMPK inhibition (Fig. 7a–c and Supplementary Fig. 8a–c), and the PINK1 preprotein remained associated with endolysosomes (Fig. 7a–c). We also imaged the same cell before and after addition of AA in the presence of insulin as a more physiological AMPK inhibitor. Again, the PINK1 reporter failed to move to mitochondria upon AA treatment and distinct PINK1 clusters remained associated with Rab7-positive endolysosomes (Supplementary Fig. 8a–c), arguing that the lack of DNAJB6 prevented their transfer to mitochondria.

In line with these observations, knockdown of DNAJB6 also prevented effective mitophagy in AA-treated neurites. Live cell imaging of YFP-Parkin recruitment to depolarized mitochondria in axons was impaired upon knockdown of DNAJB6 (Fig. 7d, e). Likewise, the recruitment of the autophagy adapter Optineurin to damaged mitochondria was significantly reduced (Fig. 7f, g). Silencing of DNAJB6 also led to a reduced colocalization of mitochondrial material with lysosomes after AA treatment (Supplementary Fig. 8d, e). Notably, these assays were all performed in the presence of insulin. This block in PINK1 activity despite active PINK1 translation (compare (Figs. 4f and 6a)) supports the following model for PINK1 import (Fig. 7h): In the absence of insulin, mitochondrial tethering of *Pink1* mRNA facilitates the co-translational import of the PINK1 preprotein, which gives rise to small translation events close to mitochondria as detected by SunTag live-cell imaging. Upon AMPK inhibition, however, PINK1 synthesis relocates from mitochondria to ribosomes near the ER and endolysosomes, and the preprotein is subsequently shuttled along the ER surface to the mitochondrial import pore via the ER chaperone DNAJB6, following the post-translational ER-SURF pathway.

Discussion

Neuronal protein translation requires the concerted action of several organelles. Neuronal mRNAs hitch-hike along several organelles, including mitochondria, early endosomes, late endosomes, and lysosomes[19,32,40–42], with a substantial portion of the transported mRNAs encoding mitochondrially targeted proteins. Furthermore, free cytosolic ribosomes are rarely observed in axons[43]. Ribosomes also hitch a ride on early endosomes[41], yet recent findings also suggest the ER-membrane as a likely source for axonal ribosomes[44,45]. Formation of organellar contact sites may enable membrane-associated ribosomes to access the transported mRNAs, as shown for endolysosomes and mitochondria[32]. However, where and how mitochondrially destined proteins are locally translated in neurons when mRNA distribution changes have remained unknown. Using a SunTag-based live-cell cytoplasmic sensor for the mitochondrial quality protein PINK1, we now uncover that PINK1 synthesis switches between mitochondrially anchored co-translational import and ER-associated post-translational import. In this post-translational state, the PINK1 preprotein utilizes the ER-SURF pathway for mitochondrial import.

The mitochondrial import pores are known to mediate post-translational import, but no mechanisms are known to prevent the premature association of the nascent chain with the TOM complex receptors. Indeed, recent proximity profiling of ribosomes close to

https://doi.org/10.1038/s41467-026-79754-5

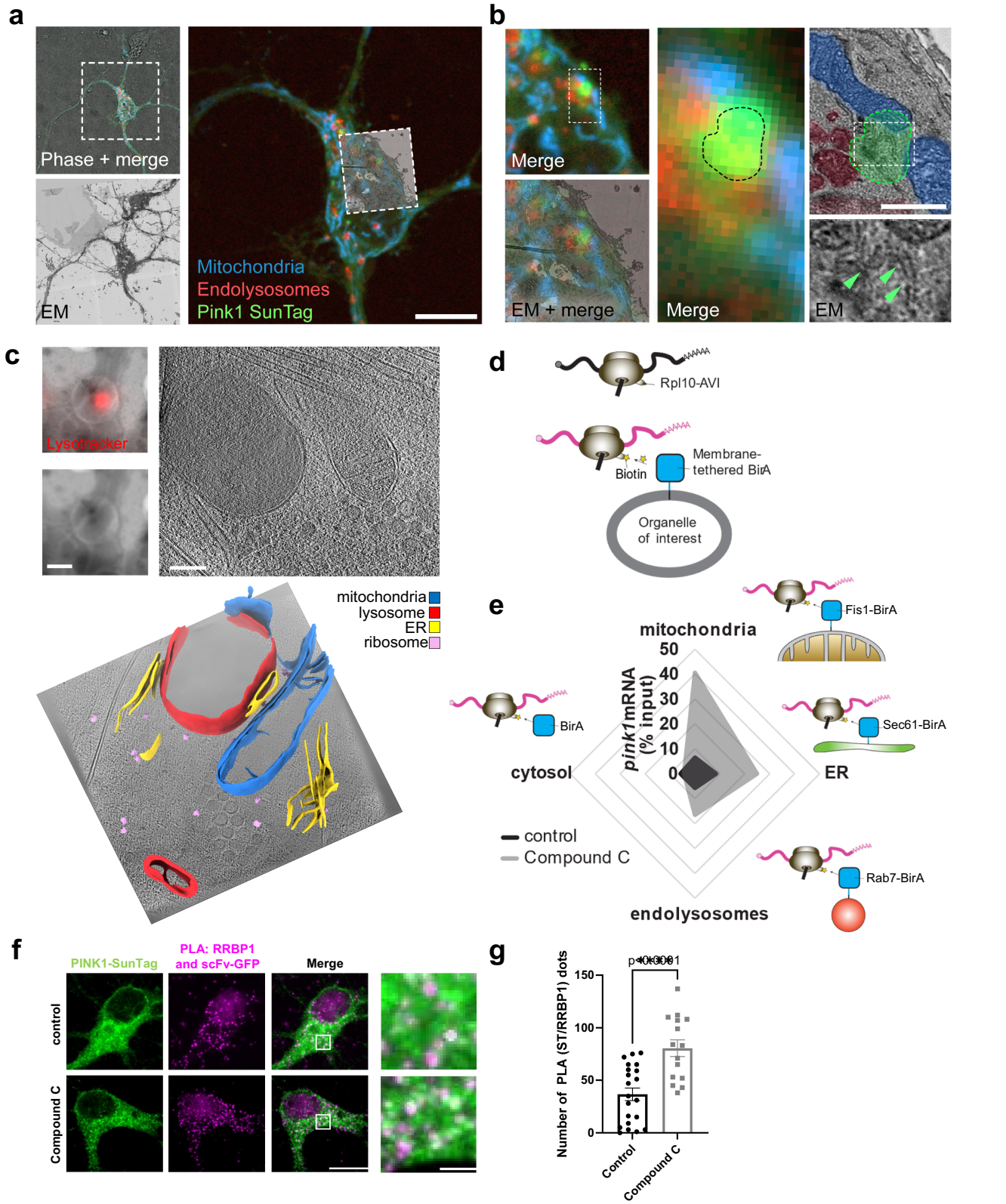

the mitochondrial surface revealed widespread co-translational import into mitochondria[22], driven either by the length of the CDS or by association of mRNAs with mitochondrially localized RBPs. During active AMPK signaling, *Pink1* mRNA is tethered to mitochondria, and this proximity would enable direct coupling of translation and import. This suggests that the mitochondrially localized PINK1 translation events we observe under control conditions (Fig. 4a, b) may correspond to co-translational import of PINK1. This is in line with the requirement of ongoing protein translation to facilitate the localization of *Pink1* mRNA with mitochondria[19]. Untethering of *Pink1* mRNA from mitochondria and subsequent translation closer to endolysosome/ER/mitochondria contact sites thus decreases the

Fig. 5 | ER tubules contribute to PINK1 biogenesis. a Correlated light and electron microscopy (CLEM) of CC-treated mouse hippocampal neurons, showing the correlation between phase, fluorescence and electron microscopy images at the cellular level. **b** Correlated light and electron microscopy (CLEM) as in (**a**) at the subcellular level. A PINK1-SunTag cluster (green) is located where two mitochondria (cyan) are in close proximity to a cluster of endolysosomes (red), and the electron micrograph (lower right inset) reveals an ER tubule within the area covered by the PINK1-SunTag signal (green arrowheads). Boxes indicate the location of insets. **c** Tomogram of a neurite of a mouse hippocampal neuron treated with CC (20 μM, 2 h), with Lysotracker-FarRed-fluorescent overlay (small upper panel left) or without it (small lower panel left) and a slide from this tomogram (right panel) showing a mature lysosome, ER tubules, mitochondria, several small vesicles and microtubules. Below is shown the segmentation of this tomogram, with the lysosomal membrane in red, ER membrane in yellow, mitochondrial membrane in blue and ribosomes in pink. For clarity, other structures are not segmented. Tomogram reconstruction is included as Supplementary Video 3. **d** Schematic representation of the BirA assay. BirA is targeted to different organelles. BirA selectively biotinylates its substrate AviTag, which is fused to the ribosomal protein Rpl10A. **e** Radar chart displaying the spatial distribution of ribosome-bound *Pink1* mRNA. The four corners represent BirA targeted to specific cellular locations: cytosol (untargeted), mitochondria (Fis1-BirA), ER (Sec61-BirA), and endolysosomes (Rab7-BirA). The distance from the center to the corners indicates the percentage of total input *Pink1* mRNA (calculated from qPCR Ct values) that is bound to ribosomes at each location. The black shape shows baseline translation in control (untreated) neurons. The gray shape shows that CC (20 μM, 2 h) treatment increases *Pink1* mRNA association with organelle-bound ribosomes, while slightly reducing the fraction on cytoplasmic ribosomes. Values represent the average of 5 independent experiments. **f** Representative images of cytosolic PINK1 clusters visualized by the SunTag system as well as the PLA signal for scFv-GFP and RRBP1 upon control (untreated) and CC (20 μM, 2 h) treatment in hippocampal neurons. Magnified insets of the indicated regions are shown to the right. **g** Quantification of the number of PLA clusters per soma as in (**f**). Unpaired two-sided Student's *t* test; $n = 15–21$ (single cells coming from 3 independent biological replicates). Data are expressed as mean (**e**) or mean ± SEM (**g**). Scale bars 10 μm for CLEM (**a**) and whole soma (**f**); 1 μm for (**b**, **c**) (small panel left); 2 μm for inset in (**f**); 100 nm for tomogram slide in (**c**).

likelihood of co-translational import of the PINK1 precursor. This may facilitate the interaction between N- and C-terminal parts of the PINK1 kinase domain post-translationally, which is necessary for the arrest of PINK1 at the TOM complex upon mitochondrial damage[46,47]. Consequently, expression of a mutant SYNJ2BP sequesters *Pink1* mRNA at mitochondria and prevents efficient PINK1 translation near endolysosomes (Fig. 2i, j and Supplementary Fig. 4g–i), delaying the initiation of mitophagy upon mitochondrial damage[20].

PINK1 maturation has already been suggested to involve mitochondria-ER contact sites in non-neuronal cells, as PINK1 mitochondrial levels are regulated by the ER-associated degradation (ERAD) machinery and especially the ATPase Valosin-containing protein (VCP)[48,49]. In that context, the interaction with the ER ensures the timely degradation of the mature PINK1 protein after its mitochondrial processing. Our data now suggest that the ER may serve a dual role, first, by storing the precursor in a chaperone-protected environment prior to import (Fig. 6a, d, e) and then, by providing part of the degradative machinery, to regulate timely destruction of the PINK1 protein. This rapid turnover of PINK1 suppresses mitophagy in the absence of mitochondrial damage. The switch between co-translational and post-translational import mechanisms for PINK1 seems specific of neurons, as in other cell types, PINK1 does not exhibit a comparable increase in translation upon AMPK inhibition (Supplementary Fig. 2k–m). We speculate that this is probably due to the differential expression of the *Pink1* mRNA RBP SYNJ2a[19]. Whether the association of PINK1 translation with membrane-localized ribosomes is observed in other cell types or represents another neuron-specific adaption to ensure the presence of ribosomes for its translation in axons will be an interesting avenue for future research.

The translation of the PINK1 protein at organellar contact sites may also serve as a means to limit the production of PINK1 during long-range transport of mitochondria into neurites. Only mitochondria that are in close apposition to endolysosomes/ER contacts will create productive PINK1 preprotein (Fig. 4d–f) capable of inducing mitophagy. This proximity ensures the timely degradation of the ensuing mitophagosome in case of mitochondrial damage. The actively degrading endolysosomes may hereby supply amino acids for efficient ER-associated translation, as recently described in non-neuronal cells[50]. Intriguingly, several amino-acyl tRNA synthetases are also located close to mitochondria and specifically interact with SYNJ2BP[35], placing them in close proximity to the lysosome-derived amino acids at such organellar contact sites.

The ER may supply chaperones to safeguard the PINK1 preprotein from aggregation on its route to mitochondria, analogous to the ER-SURF pathway observed in yeast[24]. We have confirmed an essential role for DNAJB6, the mammalian homolog of the chaperone Djp1, for PINK1 function in neurons (Figs. 6 and 7). Transfer of the ER-localized PINK1 precursor presumably occurs at a mitochondria-ER contact site. We observe the PINK1 precursor in close proximity to RRBP1 upon untethering of the SYNJ2a-SYNJ2BP interaction (Fig. 5f, g), yet silencing RRBP1 still allowed PINK1 activity at mitochondria (Supplementary Fig. 6f, g), suggesting that other mitochondria-ER contact sites can circumvent the loss of RRBP1-SYNJ2BP interaction. This is in line with the current model of the ER-SURF pathway in yeast, in which loss of multiple mitochondria-ER contact sites is necessary to abolish this type of mitochondrial import pathway[37].

DNAJB6 has been previously implicated in PINK1/Parkin-mediated mitophagy, demonstrated by its ability to overcome the failure of a Parkin RING domain mutant (C289G). This rescue is likely attributed to its function as a disaggregase for this aggregation-prone Parkin mutant[51]. Similarly, its overexpression can reduce the toxicity of other aggregation-prone proteins, including alpha-synuclein and Huntingtin[52,53], and DNAJB6 is even found at the core of Lewy bodies, the pathological hallmark of PD[54]. Our identification of DNAJB6 as a crucial factor in PINK1 import provides a connection between these aggregates and mitochondrial quality control. It is conceivable that sequestration of DNAJB6 into Lewy bodies might diminish the available pool for ER-SURF of the PINK1 protein precursor, consequently affecting mitochondrial quality control. As our results are mainly derived from in vitro cultured mouse neurons that do not develop Lewy body pathologies, future studies will be needed to confirm this hypothesis. By elucidating the locally active mechanisms governing mitochondrial protein translation and targeting in neurons, novel approaches to improve mitochondrial biogenesis and quality control could emerge.

Methods

Mouse primary hippocampal and cortical neurons

Mouse primary hippocampal and cortical neurons were obtained from embryonic day 16.5 (E16.5) embryos of timed-pregnant mice as previously described[19,20]. The mouse procedures in this study received approval from the Government of Upper Bavaria and were conducted in accordance with relevant guidelines and regulations. C57BL/6 WT mice were housed in the animal facility of the Max Planck Institute for Biological Intelligence, Martinsried, Germany. The animals were provided with a controlled environment (20–24 °C, 45%–65% humidity, 14:10 h light/dark cycle) including unrestricted access to regular chow diet and water. Enrichment was provided in the form of a cardboard house, a wooden plank with three holes and two types of nesting material. Brain tissue from E16.5 embryos of both sexes was pooled

https://doi.org/10.1038/s41467-026-79754-5

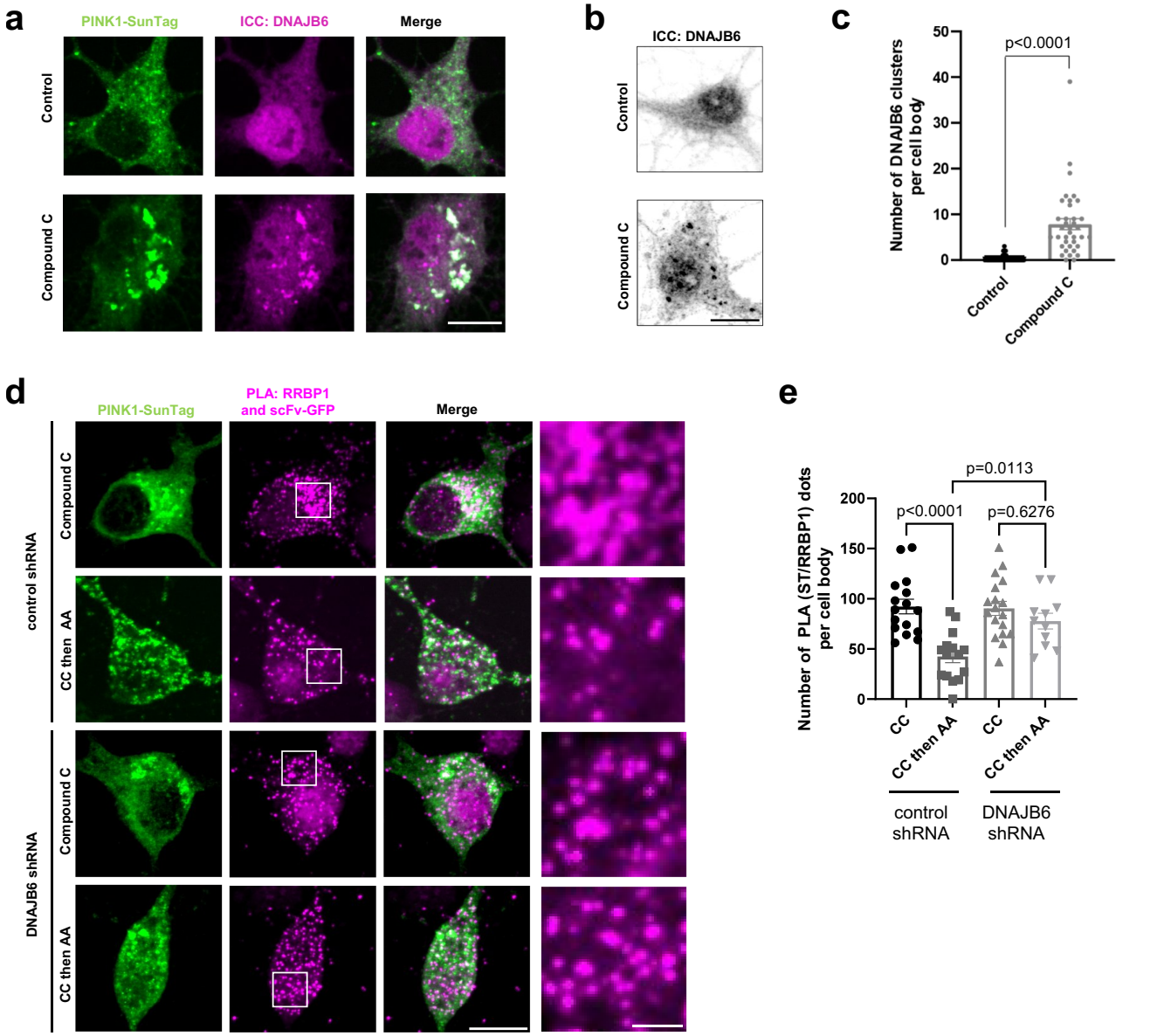

Fig. 6 | PINK1 requires DNAJB6 to exit the ER-associated clusters. **a** Representative images of cytosolic PINK1 protein clusters visualized by the SunTag system and immunostaining against endogenous DNAJB6 upon control (untreated) or CC (20 μM, 2 h) treatment in hippocampal neurons. **b** Representative images of DNAJB6 immunostaining upon control (untreated) or CC (20 μM, 2 h) treatment in hippocampal neurons. **c** Quantification of the number of DNAJB6 clusters per cell body as in (**b**). Unpaired two-sided Student's *t* test; $n = 37–44$ (single cells coming from 3 independent biological replicates). **d** Representative images of cytosolic PINK1 clusters visualized by the SunTag system as well as the PLA signal for scFv-GFP and RRBP1 upon CC (20 μM, 2 h) and AA (20 μM, 45 min) treatment in hippocampal neurons that express either control or DNAJB6 shRNA. Magnified insets of the indicated regions are shown to the right. AA addition causes a clear reduction in number of PLA dots in CC-treated control neurons as PINK1 leaves the ER (RRPB1), which is suppressed by DNAJB6 knockdown. **e** Quantification of the number of PLA dots per soma as in (**d**). One-way ANOVA followed by Tukey's post hoc test; $n = 15–18$ (single cells coming from 3 independent biological replicates). Data are expressed as mean ± SEM. Scale bars, 10 μm for whole soma, 2 μm for insets.

without prior sex determination, and primary neurons derived from these pooled tissues were used for experiments.

The timed-pregnant mice were euthanized using CO_2 followed by the rapid extraction of the E16.5 embryos from the uterus. The embryos were placed into ice-cold dissociation medium (Ca^{2+}-free Hank's Balanced Salt Solution with 10 mM $MgCl_2$, 1 mM kynurenic acid, and 10 mM HEPES). After removal from the amniotic sac, the embryos were immediately decapitated using forceps. Under a dissecting microscope, the brains were extracted from the skull followed by removal of the cerebellum, the midbrain and the meninges resulting in the isolation of the two cortices. From each hemisphere, the hippocampus was dissected, and the collected hippocampi and cortices were placed in distinct tubes containing ice-cold dissociation medium. To enzymatically dissociate the tissue, papain/L-cysteine (Sigma-Aldrich) was applied and after a 5-min incubation at 37 °C stopped by addition of trypsin inhibitor (Abnova). Subsequently, the tissue underwent three washes with NB + B27 + PSG medium [Neurobasal medium containing B27, 500 μg/ml L-glutamine, and 100 U/ml penicillin/100 μg/ml streptomycin (1% P/S) (all from Thermo Fisher Scientific)]. Finally, the hippocampal and cortical tissues were separately dissociated into single cells through trituration (10–15 times) using a p1000 pipette-tip. Hippocampal and cortical neurons were

https://doi.org/10.1038/s41467-026-79754-5

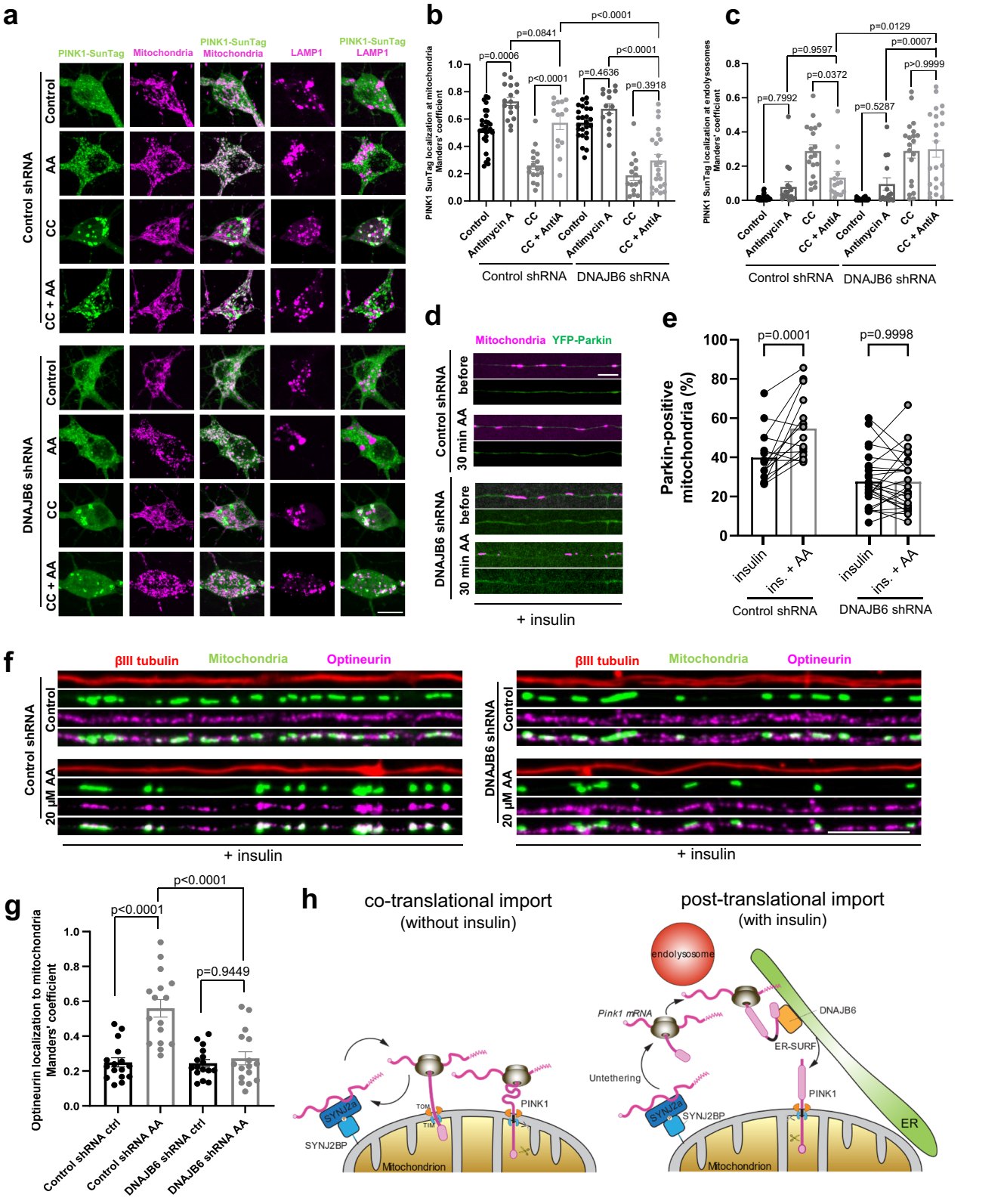

seeded on 24-well glass bottom plates (CellVis), on acid-washed glass coverslips (No. 1.5H, Marienfeld) or on 6-well plates (Greiner), which were coated with 3.5 μg/ml laminin (Thermo Fisher Scientific) and 20 μg/ml poly-L-lysine (PLL; Sigma-Aldrich), and cultivated in NB + B27 + PSG. The primary neurons were maintained in a humidified incubator with 5% CO_2 at 37 °C. Half of the medium was replaced with fresh NB + B27 + PSG every three to 5 days.

Human induced pluripotent stem cell (iPSC)-derived cortical neurons

Human induced pluripotent stem cells (iPSCs; cell line HPSI0314-hoik_1) were acquired from the Wellcome Trust Sanger Institute HipSci Repository. The cells were cultured in StemFlex medium (Thermo Fisher Scientific) in 10 cm dishes (Falcon) coated with Matrigel (Corning). The StemFlex medium was daily renewed, and

Fig. 7 | Loss of DNAJB6 impairs PINK1-dependent mitophagy. a Representative images of cytosolic PINK1 protein clusters visualized by the SunTag system and fluorescently-labeled organelles (mito-BFP and LAMP1-mCherry) in the soma of hippocampal neurons expressing control or DNAJB6 shRNA. The neurons were treated with vehicle (control) or AA (20 μM, 45 min), with or without CC pre-treatment (20 μM, 1 h). **b** Quantification of the Manders' coefficient of the colocalization between the PINK1-SunTag signal and the mitochondrial signal as in (**a**). One-way ANOVA followed by Tukey's post hoc test; $n = 14–28$ (single cells coming from 4 independent biological replicates). **c** Quantification of the Manders' coefficient of the colocalization between the PINK1-SunTag signal and the endolysosomal signal as in (**a**). One-way ANOVA followed by Tukey's post hoc test; $n = 14–28$ (single cells coming from 4 independent biological replicates). **d** Representative images of axons overexpressing YFP-Parkin (green) and mito-BFP (magenta) together with either control shRNA or DNAJB6 shRNA expressing plasmids, before and after AA (20 μM, 30 min) treatment in medium containing 100 μg/ml insulin. **e** Quantification of mitochondrial Parkin recruitment as in (**d**). Two-way ANOVA followed by Šídák's multiple comparisons test; $n = 16–26$ (single cells coming from 4 independent biological replicates). **f** Representative images of neurites of hippocampal neurons overexpressing mito-meGFP as well as either control shRNA or DNAJB6 shRNA in insulin-containing NB + B27 medium. The neurons were treated with vehicle (control) or AA (20 μM, 45 min) and immunostained against optineurin and βIII tubulin. **g** Quantification of the Manders' coefficient of the colocalization between the optineurin and the mitochondrial signal as in (**f**). One-way ANOVA followed by Tukey's post hoc test; $n = 16$ (single cells coming from 3 independent biological replicates). **h** Schematic illustrating PINK1 biogenesis in neurons. Left: In the absence of insulin, *Pink1* mRNA is tethered to the mitochondrial outer membrane via SYNJ2a/SYNJ2BP, facilitating direct co-translational import of PINK1 into mitochondria through the TOM/TIM complexes. Right: In the presence of insulin or upon AMPK inhibition, *Pink1* mRNA untethers and PINK1 synthesis relocates from mitochondria to ribosomes near the ER and endolysosomes. The resulting PINK1 preprotein is captured at the ER surface by the chaperone DNAJB6 and shuttled via the ER-SURF pathway to mitochondria for post-translational import. Data are expressed as mean ± SEM (**b, c, g**) or mean (**e**). Scale bars, 10 μm for whole soma and neurites (**a, f**) or 5 μm (**d**).

iPSCs were passaged at 80% confluency using the enzyme-free passaging reagent ReLeSR (Stem Cell Technologies).

To induce the differentiation of iPSCs into cortical neurons, the previously described protocol involving the overexpression of the transcription factor neurogenin-2 (NGN-2) was used[20,55]. Briefly, on day −2, iPSCs were dissociated into single cells using Accutase (Thermo Fisher Scientific) and seeded in 10 cm dishes coated with Matrigel at a density of 2.5×10^6 cells per dish in StemFlex medium containing 10 μM Y-27632 (Tocris). Twenty-four hours after seeding, on day −1, the cells underwent lentiviral transduction with FudeltaGW-rtTA and pLV-TetO-hNGN2-eGFP-puro in StemFlex medium, which are essential for subsequent differentiation into cortical neurons. Following a 5-h incubation, the medium was exchanged with fresh StemFlex supplemented with 2 μg/ml doxycycline (Takara) to initiate TetO gene expression. On day 0, the cells were exposed to N2/DMEM/F12/NEAA (N2 medium; Thermo Fisher Scientific) containing 2 μg/ml doxycycline, 10 ng/ml NT-3 (PeproTech), 0.2 μg/ml laminin (Thermo Fisher Scientific) and 10 ng/ml BDNF (PeproTech). On day 1, a 24-h Puromycin selection phase was initiated by introducing fresh N2 medium containing 1 μg/ml Puromycin (Enzo Life Sciences), 2 μg/ml doxycycline, 10 ng/ml NT-3, 0.2 μg/ml laminin, and 10 ng/ml BDNF to the cells. On day 2, the transition from N2 medium to B27/Neurobasal-A/Glutamax (B27 medium; Thermo Fisher Scientific) took place, supplemented with 2 μg/ml doxycycline, 10 ng/ml NT-3, 0.2 μg/ml laminin, 10 ng/ml BDNF, and 2 μM Ara-C (Sigma-Aldrich). From day 3 to 6, medium replacement occurred every other day (day 3 and 5) using fresh B27 medium supplemented with 2 μg/ml doxycycline, 10 ng/ml NT-3, 0.2 μg/ml laminin, 10 ng/ml BDNF, and 2 μM Ara-C. On day 7, the B27 medium was replaced by conditioned Südhof neuronal growth medium (NGN2 glial conditioned medium/B27/Neurobasal-A/$NaHCO_3$/Glucose/Transferrin/L-Glutamine) containing 10 ng/ml NT-3, 0.2 μg/ml laminin, and 10 ng/ml BDNF. Additionally, the medium was supplemented with 10 μM Y-27632 to prime the cells for re-plating. The re-plating of iPSC-derived cortical neurons took place on day 8, involving cell dissociation using TrypLE Express (Thermo Fisher Scientific) for 5 min at 37 °C. Following enzyme inactivation using fetal bovine serum (FBS; Thermo Fisher Scientific), a 5-min centrifugation at 200 × *g*, and resuspension in fresh conditioned Südhof neuronal growth medium containing 10 ng/ml NT-3, 0.2 μg/ml laminin and 10 ng/ml BDNF, the cells were filtered through a 70 μm cell strainer. Subsequently, the cells were seeded on 6-well plates (Greiner) or on acid-washed glass coverslips (No. 1.5H, Marienfeld) at a density of 2×10^6 or 10^5 cells per well, respectively. Human iPSC-derived neurons were maintained in a humidified incubator with 5% CO_2 at 37 °C. Half of the medium was replaced with fresh conditioned Südhof neuronal growth medium supplemented with 10 ng/ml NT-3, 0.2 μg/ml laminin and 10 ng/ml BDNF every other day.

HEK293T and HeLa cells

Human embryonic kidney 293-T (HEK293T) and Henrietta Lacks cervical carcinoma (HeLa) cells were obtained from ATCC® (Cat No.CRL-11268G-1, RRID:CVCL_UE07, and Cat# 300194/p772_HeLa, RRID:CVCL_0030). They were cultured in T75 flasks (Falcon) using Dulbecco's modified Eagle medium (DMEM) containing Glutamax (Thermo Fisher Scientific), 10% FBS and 1% P/S. HEK293T and HeLa cells were maintained in a humidified incubator at 37 °C with 5% CO_2. Passaging of cells was performed twice a week at approximately 80% confluency utilizing Trypsin-EDTA (Thermo Fisher Scientific). Experiments were performed until cells reached passage 15–20.

DNA constructs

Mito-meGFP, mito-mRaspberry-7, mito-BFP, mCherry-Rab7A, pLAMP1-mCherry, TMEM192-mRFP-3xHA, nls-ha-MCP-VenusN-nls-ha-PCP-VenusC, scFv-GCN4-sfGFP (scFv-sfGFP), AviTag-RPL10a and YFP-Parkin were purchased from Addgene (#172481, #55931, #49151, #61804, #45147, #134631, #52985, #60907, #62365, and #23955, respectively). The plasmids required for neuronal differentiation of iPSCs FudeltaGW-rtTA and pLV-TetO-hNGN2-eGFP-puro, as well as the plasmids for virus production pMDLg/pRRE, pMD2.G, and pRSV-Rev were acquired from Addgene as well (#19780, #79823, #12251, #12259, and #12253, respectively). A non-targeting control shRNA plasmid (SHC016) as well as the plasmids coding for an shRNA against DNAJB6 (TRCN0000008559), RRBP1 (TRCN0000194406) or PINK1 (TRCN0000026743) in a pLKO vector backbone were purchased from Sigma-Aldrich.

Pink1-kinase dead-MS2-PP7 and myc-tagged SYNJ2BP-WT[19] as well as myc-tagged SYNJ2BP-S21E[20] plasmids have been previously described. The Pink1-kinase dead-10xGCN4$_{mito}$–12xMS2-PP7 (Pink1-SunTag$_{mito}$) and Pink1-kinase dead-10xGCN4$_{cyto}$–12xMS2-PP7 (PINK1-SunTag$_{cyto}$) were generated by inserting 10x GCN4 consecutive repeats (obtained by enzymatic restriction) in frame between the amino acid positions 50–56 or 141–145 of rat PINK1, respectively. The construct expressing PINK1-SunTag$_{cyto}$-ODD was generated by inserting 2 times in tandem the oxygen degradation domain (ODD; LDLEMLAPYIPMDDDFQL) of mouse HIF1alpha (corresponding to Proline-577) at the C-terminus of PINK1-SunTag$_{cyto}$. The primers coding for the ODD were synthesized in vitro (Eurofins). Compatible target positions were generated at the indicated positions by site directed mutagenesis by PCR using Q5 High-Fidelity DNA Polymerase (NEB). Constructs were grown on Stbl3 chemically competent *E. coli*

bacteria (Thermo Fisher Scientific). The scFv-GCN4-mRaspberry (scFv-mRaspberry) and the scFv-GCN4-mScarlet (scFv-mScarlet) were generated by substituting the sfGFP coding sequence of the scFv-GCN4-sfGFP plasmid by the mRaspberry coding sequence (obtained from mito-mRaspberry-7 plasmid) or the mScarlet coding sequence (obtained from a mito-mScarlet plasmid). Plasmids were enzymatically digested and corresponding fragments were ligated by T4 ligase activity (NEB). The BirA-mCherry-Sec61β construct was generated by PCR amplification of the BirA-mCherry-Sec61β, including the Tet-O inducible promoter, from the Addgene plasmid #62366 followed by its insertion into the lentiviral vector backbone pMK1047 of the Addgene construct #62365 using the restriction enzymes NheI and EcoRI. The BirA-mCherry-Fis1 construct was generated by first replacing Sec61β coding sequence in the Addgene construct #62366 by the C-terminal part of Fis1 using restriction-free cloning[56]. Afterwards, BirA-mCherry-Fis1, including the Tet-O inducible promoter was amplified and subsequently inserted into the vector backbone pMK1047 of the Addgene plasmid #62365 as before. The BirA-mCherry-Rab7A construct was generated by amplifying BirA-mCherry, including the Tet-O inducible promoter from the Addgene plasmid #62366 and Rab7A from the Addgene plasmid #61804. In a three-way ligation, both inserts were integrated into the vector backbone pMK1047 of the Addgene plasmid #62365 using the restriction enzymes NheI, SbfI, and EcoRI. Cytosolic BirA-mCherry construct was generated by amplifying BirA-mCherry, including the Tet-O inducible promoter from the Addgene plasmid #62366, including a stop codon by site directed mutagenesis by PCR. The PCR product was then inserted into the vector backbone pMK1047 of the Addgene plasmid #62365 using the restriction enzymes NheI and EcoRI. Constructs were grown on DH5α chemically competent *E. coli* bacteria (strain Invitrogen, prepared in-house).

Lentivirus production

Lentiviral particles were generated using HEK293T cells as previously described[20]. The cells were seeded onto collagen type-I (Sigma-Aldrich)-coated 10 cm dishes (Falcon) at a density of 6×10^6 cells per dish and cultured in DMEM containing 10% FBS and 1% P/S. After 24 h, each 10 cm dish of HEK293T cells underwent transfection with 5 μg of the packaging plasmid mix (pMDLg/pRRE, pRSV-Rev, pMD2.G; ratio 4:1:1) and 5 μg of the relevant transfer plasmid (pLV-TetO-hNGN2-eGFP-puro, FudeltaGW-rtTA, AviTag RPL10a, BirA-mCherry-Fis1, BirA-mCherry-Sec61β, BirA-mCherry-Rab7A, cytosolic BirA-mCherry) using TransIT-Lenti reagent (Mirus Bio). After 48 h, the cell culture medium containing lentiviral particles was harvested, clarified by centrifugation at 300 × *g* for 10 min at room temperature, and then mixed with lentivirus precipitation solution (Alstem) at a 4:1 ratio. The mixture was incubated at 4 °C overnight before undergoing centrifugation at 1500 × *g* for 30 min at 4 °C to precipitate lentiviral particles. After discarding the supernatant, the pellet containing lentiviral particles was reconstituted in 1 ml of ice-cold PBS per 10 cm dish, aliquoted and stored at −80 °C.

Immunoblotting

For the cycloheximide chase assay, human iPSC-derived neurons were seeded in 6-well plates (Greiner) coated with PLL and laminin at a density of 2×10^6 cells per well and cultured in conditioned Südhof neuronal growth medium as described above. On day in vitro 14 (DIV14), the neurons were pre-incubated in medium with or without insulin for 2 h followed by 70 μM cycloheximide (Enzo Life Sciences) treatment for 30, 60, or 120 min. Subsequently, the neurons were lysed using a buffer containing 25 mM Tris/HCl pH 7.4, 1% NP-40, 150 mM NaCl, supplemented with 1x protease inhibitor cocktail (Roche) and 200 μM PMSF. After centrifugation of the lysates at 9300 × *g* for 1 min at 4 °C, the pellet was discarded while the supernatant was mixed with Laemmli sample buffer and boiled at 95 °C for 5 min. Using standard protocols, the samples were electrophoretically separated by SDS-PAGE (12 % polyacrylamide gel) and immunoblotted on Nitrocellulose membranes (Amersham/Cytiva). Membranes were blocked with 1X Blocker FL fluorescent Blocking Buffer (Thermo Fisher Scientific). Antibodies employed for immunoblotting included anti-PINK1 rabbit antibody (1:500; Novus Biologicals, #BC100-494) and anti-βIII tubulin mouse (2G10) antibody (1:2,000; Invitrogen, #MA1-118).

For the validation of RRBP1 and DNAJB6 shRNAs, HEK293T cells were seeded in 6-well plates (Greiner) at a density of 0.5×10^6 cells per well and cultured in DMEM containing 10% FBS and 1% P/S. One day after seeding, transfection was performed using calcium phosphate for 5 h introducing control shRNA, shRNA targeting RRBP1 or DNAJB6 into the cells. Three days after transfection, HEK293T cells were lysed using a buffer containing 25 mM Tris/HCl pH 7.4, 1% NP-40, 150 mM NaCl, supplemented with 1x protease inhibitor cocktail (Roche) and 200 μM PMSF. After centrifugation of the lysates at 9300 × *g* for 1 min at 4 °C, the pellet was discarded while the supernatant was mixed with Laemmli sample buffer and boiled at 95 °C for 5 min. Using standard protocols, the samples were electrophoretically separated by SDS-PAGE (12% polyacrylamide gel) and immunoblotting. Antibodies employed for immunoblotting included anti-RRBP1 rabbit antibody (1:500; Abcam; #ab95983), anti-DNAJB6 rabbit antibody (1:500; Proteintech; #11707-1-AP) and anti-β-actin mouse (AC-74) antibody (1:500; Sigma-Aldrich, #A5316).

For the analysis of the cellular localization and processing of PINK1-SunTag$_{mito}$ and PINK1-SunTag$_{cyto}$, HEK293T cells were transfected with the indicated plasmids using standard calcium phosphate protocols. After 24–36 h of transfection, cells were incubated with either control medium or medium containing either 100 μM Carbonyl cyanide m-chlorophenyl hydrazone (CCCP; Sigma) or 10 μM MG-132 (Sigma) for 2 h. Then, cells were collected, and mitochondrial fractions were isolated using a previously reported protocol[57]. Briefly, cell membranes were physically broken with a douncer in 500 μl detergent-free buffer A (20 mM HEPES, 220 mM Mannitol, 70 mM Sucrose, 1 mM EDTA, 2 mg/ml BSA) and lysates were centrifuged at 200 × *g* for 5 min at 4 °C in a swing-rotor. Supernatants were collected (total lysate) and centrifuged at 12,000 × *g* for 10 min at 4 °C. Supernatants were discarded and the pellet containing the crude mitochondrial fraction was resuspended in 100 μl buffer B (20 mM HEPES, 220 mM Mannitol, 70 mM Sucrose, 1 mM EDTA) and centrifuged at 12,000 × *g* for 15 min at 4 °C. Pellets were resuspended in either 100 μl buffer B alone or containing 3 μl thermosensitive Proteinase K (NEB) and incubated at 4 °C for 30 min. PK was inactivated at 65 °C for 15 min. Supernatants were mixed with Laemmli sample buffer and incubated at 65 °C for 10 min. Samples were electrophoretically separated by SDS-PAGE (10% polyacrylamide gel) and immunoblotted on Nitrocellulose membranes. Antibodies employed for immunoblotting included anti-GCN4 rabbit antibody (1:10,000; Novus, #NBP2-81274) and anti-ATP5α mouse antibody (1:1000; Invitrogen, #43-9800).

For the analysis of the treatments on general translation, we used DIV8 mouse cortical neurons (6×10^6 cells/condition). Cells were incubated for 2 h with either control NB + B27 + PSG medium, Hibernate-E, or Hibernate-E containing 20 μM CC. During the last 30 min, 10 μg/ml puromycin was added to the culture medium. Cells were then lysed using a lysis buffer (50 mM Tris-HCl, 150 mM NaCl, 0.5% Triton X-100) supplemented with 1% complete protease inhibitor, 1% SDS and 2.5 U/μl Benzonase (MERCK; E1014). Samples were electrophoretically separated by SDS-PAGE gels, and immunoblots were developed using an anti-puromycin mouse antibody (1:1000; EQ0001; Kerafast) and anti-βIII tubulin mouse (2G10) antibody (1:2000; Invitrogen, #MA1-118).

In all cases, secondary antibodies anti-mouse or anti-rabbit Fc chains generated in either goat or donkey were fluorescently

conjugated with either A488 or A647, and detected with an iBright imaging system (Thermo Fisher Scientific). Uncropped versions of the blots are provided in Supplementary Fig. 9.

Live cell mRNA imaging

Live cell imaging of *Pink1* mRNA in mouse primary hippocampal neurons was performed as described previously[19,20]. Neurons were seeded in 24-well glass bottom plates (CellVis) coated with PLL and laminin at a density of 1–1.5 × 10^5 cells per well and cultured in NB + B27 + PSG as described above. On DIV7, transfection was performed with Lipofectamine® 2000 transfection reagent (Thermo Fisher Scientific) introducing 4 μg of Pink1-SunTag$_{cyto}$ and 1 μg of nls-ha-MCP-VenusN-nls-ha-PCP-VenusC along with 0.3 μg of TMEM192-mRFP-3xHA or 0.3 μg of scFv-mRaspberry into the neurons. On DIV9, the neuronal medium was exchanged with Hibernate E medium without phenol red (BrainBits) and the neurons were incubated with 20 μM Compound C (CC; Abcam, 2 h) or 500 nM insulin (Sigma-Aldrich, 1 h). Afterwards, the neurons were imaged at the Imaging Facility of the Max Planck Institute for Biological Intelligence, Martinsried, Germany, using an Eclipse Ti2 spinning disk microscope (Nikon) with a Photometrics Prime BSI Scientific CMOS camera (Teledyne Vision Solutions), a 60×/NA 1.2 oil immersion objective as well as the NIS-Elements software (version 5.21.03).

For the co-visualization of *Pink1* mRNA and protein by live-cell imaging, mouse hippocampal neurons were grown on PLL and laminin coated glass bottom plates. On DIV9 neurons were co-transfected with 1 μg PINK1-SunTag-$_{cyto}$, 0.2 μg MCP-PCP-split-YFP, 0.2 μg scFv-GCN4-mScarlet and 0.2 μg mito-BFP using Lipofectamine® 2000, as described above. On DIV20, imaging was performed in Hibernate E medium (BrainBits), at the Eclipse Ti2 Spinning disk microscope, as before. The same neuron was imaged before and after stimulation with 100 μg/ml insulin (I9278; Sigma) for 1 h.

For visualization of the PINK1-SunTag$_{cyto}$-ODD, mouse hippocampal neurons were grown on PLL and laminin coated glass bottom plates, and co-transfected with 1 μg PINK1-SunTag$_{cyto}$-ODD and 0.2 μg scFv-GCN4-sfGFP using Lipofectamine® 2000, as described above. Neurons were imaged in Hibernate-E, as indicated, 2–3 DIV after transfection using an Eclipse Ti2 Spinning disk microscope, as before. Same neurons were imaged before and 1 h after adding 20 μM CC or 100 μg/ml insulin (I9278; Sigma).

Proximity ligation assay

Mouse primary hippocampal neurons were seeded on acid-washed glass coverslips (No. 1.5H, Marienfeld) coated with PLL and laminin at a density of 5 × 10^4 cells per well and cultured in NB + B27 + PSG as described above. For detecting a PLA signal between the PINK1 SunTag signal (scFv-sfGFP) and the ribosomes, RRBP1 or Sec61β, on DIV5 primary neurons were transfected with 0.25 μg of scFv-sfGFP, with or without 1 μg PINK1-SunTag$_{cyto}$, and with or without 0.3 μg control shRNA or DNAJB6 shRNA (depending on the experiment) using Lipofectamine® 2000 transfection reagent (Thermo Fisher Scientific). On DIV7, the neurons were incubated with or without 20 μM CC (Abcam) for 2 h and with or without 20 μM Antimycin A (AA, Sigma-Aldrich; 45 min), followed by fixation using 4% warm PFA for 15 min at room temperature. The neurons were permeabilized in 0.3% Triton X-100/PBS for 10 min and the next steps were conducted following the manufacturer's guidelines (Sigma-Aldrich) and as previously described[19,20]. Neurons were first incubated with the Duolink blocking solution for 60 min at 37 °C in a humidity chamber and afterwards with the primary antibody anti-RPS6 rabbit (5G10) (1:200; Cell Signaling Technology, #2217), anti-RRBP1 rabbit (1:500; Abcam, #ab95983) or anti-Sec61β rabbit (1:500; Proteintech, #15087-1-AP) diluted in Duolink antibody diluent at 4 °C overnight. The expressed scFv-sfGFP serves as the second primary antibody (mouse) inside the cells. One of the control samples was incubated without the anti-RPS6 antibody. On the following day, cells underwent two 5-min washes at room temperature with buffer A (0.01 M Tris, 0.15 M NaCl, 0.05% Tween 20) followed by incubation with the Duolink anti-rabbit minus and anti-mouse plus PLA probes, diluted in a 1:5 ratio in the Duolink antibody diluent, for 60 min at 37 °C. After another two 5-min washes with buffer A at room temperature, a ligase, diluted in a 1:40 ratio in the Duolink ligation buffer, was added to the cells for 30 min at 37 °C. Afterwards, cells were washed twice for 5 min with buffer A at room temperature and subsequently treated with a polymerase, diluted in a 1:80 ratio in the Duolink amplification buffer containing fluorescently-labeled oligonucleotides (Cy5) for 100 min at 37 °C. After two 10-min washing steps in buffer B (0.2 M Tris, 0.1 M NaCl) and a final 1-min washing step in 0.01x buffer B at room temperature, Fluoromount G (Invitrogen) was used to mount the coverslips. The coverslips were imaged at the Imaging Facility of the Max Planck Institute for Biological Intelligence, Martinsried, Germany, using an Eclipse Ti2 spinning disk microscope (Nikon) with a Photometrics Prime BSI Scientific CMOS camera (Teledyne Vision Solutions), a 60×/NA 1.2 oil immersion objective as well as the NIS-Elements software (version 5.21.03). To control for variability in transfection efficiency, an independent fluorescent plasmid was co-transfected as a baseline expression marker. Neurons were screened prior to image acquisition, and only cells displaying comparable, moderate intensity for this co-transfection marker were selected for imaging across all experimental conditions.

Protein translation assays

SunTag system. Mouse primary hippocampal neurons were seeded in 24-well glass bottom plates (CellVis) coated with PLL and laminin at a density of 1–1.5 × 10^5 cells per well. HeLa cells were seeded in 24-well glass bottom plates (CellVis) at a density of 5 × 10^4 cells per well. Cells were cultured in their respective media, as described above. On DIV7 or DIV9, neuronal transfection was performed with Lipofectamine® 2000 transfection reagent (Thermo Fisher Scientific) introducing 1 μg PINK1-SunTag$_{mito}$ or PINK1-SunTag$_{cyto}$ and 0.25 μg of scFv-sfGFP along with 0.3 μg of the respective organellar markers (mito-BFP, mito-mRaspberry, mCherry-Rab7A, TMEM192-mRFP-3xHA or pLAMP1-mCherry) and, when indicated, 0.3 μg of plasmids encoding mycSYNJ2BP-WT or -S21E, control shRNA, DNAJB6 shRNA or RRBP1 shRNA into the neurons. One day after seeding, HeLa cells were transfected with 1 μg PINK1-SunTag$_{cyto}$ and 0.25 μg of scFv-sfGFP using calcium phosphate. On DIV9-DIV12 or two days after transfection, the neuronal and HeLa cell medium, respectively, was exchanged with Hibernate E medium without phenol red (BrainBits) and the cells underwent the following treatments: 20 μM CC (Abcam, 2 h), 1 mM AICAR (Abcam; 2 h), 500 nM insulin (Sigma-Aldrich; 1 h),1 μM Wortmannin (EMD Millipore; 2 h), 20 μM Antimycin A (AA, Sigma-Aldrich; 2 h), or 100–200 μg/ml Puromycin (Enzo Life Sciences; 30 min–2 h). Afterwards, the neurons and HeLa cells were imaged live at the Imaging Facility of the Max Planck Institute for Biological Intelligence, Martinsried, Germany, using an Eclipse Ti2 spinning disk microscope (Nikon) with a Photometrics Prime BSI Scientific CMOS camera (Teledyne Vision Solutions), a 60×/NA 1.2 oil immersion objective as well as the NIS-Elements software (version 5.21.03). Cells were kept at a controlled temperature of 37 °C during the imaging session. To control for expression level variability across transfected cells, cells were selected prior to imaging by evaluating the fluorescence signal of the co-transfected, reporter-unrelated organellar marker channel (e.g., mitochondrial or endo-lysosomal marker). Only neurons exhibiting comparable fluorescent intensity levels were imaged.

Proximity ligation assay coupled with puromycylation (puro-PLA). Human iPSC-derived neurons were seeded on acid-washed glass coverslips (No. 1.5H, Marienfeld) coated with PLL and laminin at a

density of 5×10^4 cells per well and cultured in conditioned Südhof neuronal growth medium as described above. On DIV14, the following treatments were performed: 20 μM CC (Abcam, 2 h), 1 mM AICAR (Abcam, 2 h), 500 nM insulin (Sigma-Aldrich, 1 h) or Südhof neuronal growth medium lacking insulin (2 h). Afterwards, 10 μg/ml puromycin (Enzo Life Sciences) was added to the medium of the cells for 5 min at 37 °C. To stop the puromycylation reaction, cells were briefly washed with PBS containing 1 mM $MgCl_2$, 0.1 mM $CaCl_2$, and 10 μg/ml cycloheximide (Enzo Life Sciences) followed by fixation using 4 % warm PFA for 15 min at room temperature. The proximity ligation assay was performed as described above including permeabilization, blocking, primary antibody incubation, PLA probe incubation, ligase treatment, and polymerase treatment. The following primary antibodies were used: anti-PINK1 rabbit antibody (1:1000, Novus Biologicals, #BC100-494), anti-Puromycin mouse (3RH11) antibody (Kerafast, #EQ0001). After mounting of the coverslips using Fluoromount G (Invitrogen), they were imaged at the Imaging Facility of the Max Planck Institute for Biological Intelligence, Martinsried, Germany, using an Eclipse Ti2 spinning disk microscope (Nikon) with a Photometrics Prime BSI Scientific CMOS camera (Teledyne Vision Solutions), a 60×/NA 1.2 oil immersion objective as well as the NIS-Elements software (version 5.21.03).

BirA assay. Mouse primary cortical neurons were seeded in 6-well plates (Greiner) coated with PLL and laminin at a density of 2×10^6 cells per well. On DIV1, neurons were lentivirally transduced for 5–8 h with the AviTag-RPL10a and the rtTA as well as one of the following BirA constructs: BirA-mCherry-Fis1, BirA-mCherry-Sec61β, BirA-mCherry-Rab7 or cytosolic BirA-mCherry. On DIV5, neurons were treated with 2 ng/μl doxycycline for 4 h to induce expression of the BirA constructs. Additionally, 20 μM CC (Abcam, 2 h) was added to the neurons. Subsequently, neurons were lysed using a buffer containing 25 mM Tris/HCl pH 7.4, 1% NP-40, 150 mM NaCl, supplemented with 1X protease inhibitor cocktail (Roche), 200 μM PMSF, and 0.1% RNasin (Promega). After centrifugation at 9300 × *g* for 1 min, the pellets were discarded and 10% of the supernatant was kept as input, while the remaining cell lysate was incubated with 30 μl Streptavidin-Agarose beads (Sigma-Aldrich) per sample for 40 h at 4 °C. Afterwards, the beads were washed five times in columns (MoBiTec) in a buffer composed of 20 mM Tris/HCl pH 8, 5 mM $MgCl_2$, 140 mM NaCl, 0.1% Triton X-100, 200 μM PMSF and 0.1% RNasin. The elution was performed by adding Laemmli sample buffer followed by boiling at 95 °C for 2 min.

For RNA isolation, input as well as pulldown samples were mixed with 1 ml TRIzol (Sigma-Aldrich) followed by addition of 100 μl BCP (1-Bromo-3-chloropropane) per sample. After centrifugation for 15 min at 12,000 × *g* at 4 °C, the upper aqueous phase was transferred to a new tube containing one volume BCP. After a second centrifugation for 5 min at 12,000 × *g* at 4 °C, the upper phase was mixed with 2.5 volumes of 100% ethanol, 100 μl 3 M sodium acetate and 10 μl glycogen. The samples were incubated at −20 °C for at least 30 min and then centrifuged for 20 min at 12,000 × *g* at 4 °C. The supernatant was discarded and the pellet was resuspended in 250 μl MilliQ water followed by addition of 1 ml 100% ethanol, 10 μl glycogen and 100 μl 3 M sodium acetate. After a final centrifugation of 5 min at 7500 × *g* at 4 °C, the pellet was resuspended in 20 μl RNase-free water.

The RNA samples were analyzed by RT-qPCR to determine *Pink1* transcript levels. 200 ng were used for complementary DNA (cDNA) synthesis with qScript™ cDNA SuperMix (Quantabio). The RT-qPCR assay was conducted in a Mic (magnetic induction cycler) PCR machine (Bio Molecular Systems) utilizing the PerfeCTa SYBR® Green FastMix (Quantabio). The specific primers used for the assay were as follows (5′ → 3′): Pink1 forward: AATGAGCCAGGAGCTGGTC; Pink1 reverse: GTACTGGCGCAGGGTACAG; β-actin forward: ACACTGTG CCCATCTACG; β-actin reverse: GCTGTGGTGGTGAAGCTGTAG.

Quantification of the mRNA enrichment at the indicated subcellular localizations and treatments was evaluated following the percent input method of the Ct values.

Mitophagy assays

Optineurin and phospho-ubiquitin immunostaining. Mouse primary hippocampal neurons were seeded on acid-washed glass coverslips (No. 1.5H, Marienfeld) coated with PLL and laminin at a density of 5×10^4 cells per well and cultured in NB + B27 + PSG as described above. On DIV5, transfection was performed with Lipofectamine® 2000 transfection reagent (Thermo Fisher Scientific) introducing 0.3 μg mito-meGFP as well as 0.3 μg control shRNA, RRBP1 shRNA or DNAJB6 shRNA into the neurons. On DIV8, neurons were incubated for 45 min with or without 20 μM AA (Sigma-Aldrich) followed by fixation using 4% warm PFA for 15 min at room temperature. The neurons were permeabilized in 0.3% Triton X-100/PBS for 10 min, blocked in 1% BSA/PBS for 1 h at room temperature, and finally incubated with the primary antibodies (anti-optineurin rabbit antibody (1:500, Abcam, #ab23666); anti-phospho-ubiquitin rabbit antibody (1:200, Millipore, #ABS1513-I); anti-βIII tubulin mouse (2G10) antibody (1:1000; Invitrogen, #MA1-118)) diluted in 1% BSA/PBS overnight at 4 °C. On the following day, the fixed neurons were subjected to three 5-min washes in PBS at room temperature and then incubated with the secondary fluorescent antibodies Alexa Fluor 568 goat anti-mouse and Alexa Fluor 647 goat anti-rabbit (Invitrogen, 1:500) diluted in 1% BSA/PBS for 2 h at room temperature. After additional three 5-min washes in PBS, the coverslips were mounted using Fluoromount G (Invitrogen) and imaged at the Imaging Facility of the Max Planck Institute for Biological Intelligence, Martinsried, Germany, using an Eclipse Ti2 spinning disk microscope (Nikon) with a Photometrics Prime BSI Scientific CMOS camera (Teledyne Vision Solutions), a 60×/NA 1.2 oil immersion objective as well as the NIS-Elements software (version 5.21.03).

Parkin recruitment. Parkin recruitment was analyzed as previously described[19,20], with small modifications. Mouse hippocampal neurons were grown on PLL and laminin coated glass bottom plates. On DIV9 neurons were co-transfected with 0.2 μg mito-BFP and 0.2 μg YFP-Parkin, together with 0.5 μg of either control shRNA or DNAJB6 shRNA expressing constructs using Lipofectamine® 2000, as described above. On DIV12, imaging was performed in Hibernate E medium (BrainBits) containing 100 μg/ml insulin, the neurons were live-imaged at the Imaging Facility of the Max Planck Institute for Biological Intelligence, Martinsried, Germany, using an Eclipse Ti2 spinning disk microscope (Nikon) with a Photometrics Prime BSI Scientific CMOS camera (Teledyne Vision Solutions), a 60×/NA 1.2 oil immersion objective, as well as the NIS-Elements software (version 5.21.03). Images of the same neuron were taken before and 30 min after addition of 20 μM AA.

Mitochondrial and lysosomal colocalization assay. Mouse primary hippocampal neurons were seeded in 24-well glass bottom plates (CellVis) coated with PLL and laminin at a density of 10^5 cells per well and cultured in NB + B27 + PSG as described above. On DIV6, transfection was performed with Lipofectamine® 2000 transfection reagent (Thermo Fisher Scientific) introducing 0.3 μg mito-meGFP and 0.3 μg LAMP1-mCherry as well as 0.3 μg control shRNA or DNAJB6 shRNA into the neurons. On DIV9, the neuronal medium was exchanged with Hibernate E medium without phenol red (BrainBits) and the neurons were incubated for 45 min with or without 20 μM AA (Sigma-Aldrich). Afterwards, the neurons were live-imaged at the Imaging Facility of the Max Planck Institute for Biological Intelligence, Martinsried, Germany, using an Eclipse Ti2 spinning disk microscope (Nikon) with a Photometrics Prime BSI Scientific CMOS camera (Teledyne Vision Solutions), a 60×/NA 1.2 oil immersion objective as well as the NIS-Elements software (version 5.21.03).

DNAJB6 immunostaining

Mouse primary hippocampal neurons were seeded on acid-washed glass coverslips (No. 1.5H, Marienfeld) coated with PLL and laminin at a density of 5×10^4 cells per well. HeLa cells were seeded on acid-washed glass coverslips (No. 1.5H, Marienfeld) at a density of 5×10^4 cells per well. Primary neurons and HeLa cells were cultured in NB + B27 + PSG and DMEM containing 10% FBS and 1% P/S, respectively, as described above. On DIV6, transfection of primary neurons was performed with Lipofectamine® 2000 transfection reagent (Thermo Fisher Scientific) introducing 1 μg of PINK1-SunTag$_{cyto}$ and 0.25 μg of scFv-sfGFP into the cells. On DIV8 or two days after seeding, neurons and HeLa cells, respectively, were incubated with or without 20 μM CC (Abcam) for 2 h followed by fixation using 4% PFA for 15 min at room temperature. The cells were permeabilized in 0.3% Triton X-100/PBS for 10 min, blocked in 1% BSA/PBS for 1 h at room temperature, and finally incubated with the primary antibodies (anti-DNAJB6 rabbit antibody (1:500, Proteintech, #11707-1-AP); anti-βIII tubulin mouse (2G10) antibody (1:1000, Invitrogen, #MA1-118); anti-β-actin mouse (AC-74) antibody (1:1000, Sigma-Aldrich, #A5316)) diluted in 1% BSA/PBS overnight at 4 °C. On the following day, the fixed cells were subjected to three 5-min washes in PBS at room temperature and then incubated with the secondary fluorescent antibodies Alexa Fluor 647 goat anti-rabbit and Alexa Fluor 488 goat anti-mouse (Invitrogen, 1:500) diluted in 1% BSA/PBS for 2 h at room temperature. After additional three 5-min washes in PBS, the coverslips were mounted using Fluoromount G (Invitrogen) and imaged at the Imaging Facility of the Max Planck Institute for Biological Intelligence, Martinsried, Germany, using an Eclipse Ti2 spinning disk microscope (Nikon) with a Photometrics Prime BSI Scientific CMOS camera (Teledyne Vision Solutions), a 60×/NA 1.2 oil immersion objective as well as the NIS-Elements software (version 5.21.03).

The effect of PINK1 silencing on DNAJB6 clustering was analyzed on mouse hippocampal neurons grown on PLL and laminin coated coverslips, and co-transfected with 0.2 μg GFP (cell fill), together with 0.5 μg of either control shRNA or PINK1 shRNA expressing constructs on DIV9, as above. On DIV12, culture medium was removed and cells were incubated for 2 h in Hibernate E (BrainBits) alone or containing 20 μM CC. Cells were fixed with 4% warm PFA for 10 min. Rabbit anti-DNAJB6 (Proteintech 11707-1-AP; 1:200) was incubated o/n and detected with a Donkey-anti-Rabbit–Alexa647 conjugated Antibody (Invitrogen; #31573; 1:400). Coverslips were mounted in Fluoromount G (Invitrogen), and imaged at the Imaging Facility of the Max Planck Institute for Biological Intelligence, Martinsried, Germany, using a Leica Stellaris 5 DMi8 inverted confocal microscope using a 63x/NA 1.4 oil immersion objective and point Hybrid detectors for image acquisition using LAS-X software (version 3.5.5). Images were acquired from GFP expressing cells. The number of clusters in the soma was quantified manually on maximum projection images obtained with Fiji/ImageJ.

Rps6 immunostaining

Mouse hippocampal neurons were grown on PLL and laminin coated coverslips, and transfected with 0.2 μg mito-meGFP on DIV7, as above. On DIV9, culture medium was removed and cells were incubated for 2 h in Hibernate E (BrainBits) alone or containing 20 μM CC. Cells were fixed with 4% warm PFA for 10 min, permeabilized with 0.3% Triton X-100/PBS for 15 min at room temperature and blocked for 30 min in 5% Donkey Serum/PBS, and finally incubated with the primary antibody overnight at 4 °C (Rabbit anti-Rps6; #2217S Cell Signaling; 1:200). After rinsing with PBS, they were incubated for 2 h at room temperature with Donkey-anti-Rabbit–Alexa647 conjugated Antibody (Invitrogen; #31573; 1:400), rinsed and mounted in Fluoromount G (Invitrogen), and imaged at the Imaging Facility of the Max Planck Institute for Biological Intelligence, Martinsried, Germany, using a Leica Stellaris 5 DMi8 inverted confocal microscope using a 63x/NA 1.4 oil immersion objective and point Hybrid detectors for image acquisition using LAS-X software (version 3.5.5). Images were acquired from mito-meGFP expressing cells.

Correlative light and scanning electron microscopy

For correlative imaging experiments, mouse primary hippocampal neurons were seeded on patterned 35 mm glass bottom dishes (MatTek, 14 mm glass diameter, 1.5 gridded coverslip) coated with PLL and laminin at a density of 1.5×10^5 cells per dish and cultured as described above. On DIV7, transfection was performed with Lipofectamine® 2000 transfection reagent (Thermo Fisher Scientific) introducing 1 μg of PINK1-SunTag$_{cyto}$, 0.25 μg of scFv-sfGFP, 0.3 μg of mito-BFP, and 0.3 μg of TMEM192-mRFP-3xHA into the neurons. On DIV9, imaging was performed at the Imaging Facility of the Max Planck Institute for Biological Intelligence, Martinsried, Germany, using an Eclipse Ti2 spinning disk microscope (Nikon) with a Photometrics Prime BSI Scientific CMOS camera (Teledyne Vision Solutions), a 60×/NA 1.2 oil immersion objective as well as the NIS-Elements software (version 5.21.03). Before imaging, the neuronal medium was exchanged with Hibernate E medium without phenol red (BrainBits) and the neurons underwent a 2 h treatment with 20 μM CC (Abcam). Following imaging, immediate fixation was performed using a freshly prepared 2.5% glutaraldehyde solution in 0.1 M cacodylate buffer (Science Services). The 2x fixative solution, pre-warmed to 37 °C, was added directly into the Hibernate E medium of the neurons at a 1:1 ratio. Following a 5 min incubation at 37 °C, it was replaced with 1x fixative and further incubated for 25 min on ice. Removal of the fixative involved three 5 min washes with 0.1 M cacodylate buffer on ice. Further processing was performed at the electron microscopy hub at the German Center for Neurodegenerative Diseases (DZNE), Munich, Germany. Employing a reduced osmium thiocarbohydrazide osmium (rOTO) *en bloc* staining protocol, the samples underwent a sequential series of treatments. This process involved postfixation in a solution containing 2% osmium tetroxide (Science Services), 1.5% potassium ferricyanide (Sigma-Aldrich) in 0.1 M sodium cacodylate buffer (pH 7.4; Science Services)[58]. The staining was intensified through a 45 min incubation at 40 °C with 1% thiocarbohydrazide (Sigma-Aldrich). Subsequently, the neurons underwent rinsing in water and immersion in a 2% aqueous solution of osmium tetroxide. After another wash, an additional level of contrast was achieved through an overnight incubation in a 1% aqueous solution of uranyl acetate at 4 °C, followed by an extra 2 h incubation at 50 °C. In preparation for subsequent processing steps, the samples underwent dehydration through a series of increasing ethanol concentrations and were infiltrated with LX112 (LADD). Following the curing process, the block was removed from the glass coverslip through a series of freeze-thaw cycles. The region of interest was trimmed (TRIM2, Leica) in accordance with the previously acquired grid pattern from confocal imaging. Serial sections, with a nominal thickness of 80 nm, were acquired using a 35° ultra-diamond knife (Diatome) on an ATUMtome (Powertome, RMC). These sections were collected onto carbon-coated Kapton tape (kindly provided by Jeff Lichtman and Richard Schalek), freshly treated with plasma (custom-built, based on PELCO easiGlow, adopted from M. Terasaki, U. Connecticut, CT). The tape stripes were affixed onto adhesive carbon tape (Science Services), and this assembly was then secured onto 4-inch silicon wafers (Siegert Wafer) and grounded through adhesive carbon tape stripes (Science Services). EM micrographs were acquired using an Apreo S2 SEM (Thermo Fisher Scientific) as previously described[59]. Hierarchical imaging of serial sections was achieved through initial mapping of the plastic tape stripes at low lateral resolution and capture of the entire tissue sections at a medium resolution (100-200 nm). Correlation of the region of interest was established through the integration of the grid pattern and neuronal morphology. Subsequently, micrographs of serial sections were acquired at a lateral resolution of 5 nm. To align the serial section

imaging data, a hybrid approach combining both automated and manual processing procedures was employed within Fiji TrakEM2[59]. Following the alignment, single sections containing the organellar structures of interest were chosen.

Cryo-electron tomography

The AU grids R 2/1 holey carbon (Quantifoil), were treated with an additional 10 nm carbon layer and plasma cleaned. Four grids were placed in a P35 culture plate (Falcon), and then coated with Laminin and poly-L-Lysine as before. One million dissociated mouse hippocampal neurons were plated per plate. Culture medium was refreshed every 2–3 days. On day 9, growth medium was removed and neurons were stimulated for 2 h with 20 μM Compound C (Abcam) in Hibernate-E medium (BrainBits) containing 50 nM LysoTracker Red DND-99 (Invitrogen). Then, cells were plunge-frozen using a VitroBot Mk4 (Thermo-Fischer) at 80% humidity and 30 °C. Grids were blotted from the back side only using a Teflon sheet from the frontside, and stored in liquid nitrogen.

Grids were analyzed under a LSM900 Airyscan2 microscope (Zeiss) to define the target areas, based on the presence of Lysotracker signal in thin processes crossing grid holes. Tomograms of the selected areas were then acquired in a Titan Krios G4 (Thermo Fisher Scientific) equipped with a SelectrisX energy filter and a Falcon 4 electron counting camera. More than 300 tomograms were acquired. The initial ".eer" files were re-grouped and converted to ".tif" with Relion converter[60]. Using WarpTools they were motion corrected and initial CTF-estimation was performed[61]. The corrupted tilts were removed manually using script developed by Linhua Tai (EMBL, Mahamid lab; personal communication, available upon request), and secondary CTF-estimation was performed. Defocus handedness was flipped and alignment was performed using AreTomo2 via Warp Tools wrapper[61,62]. Then, the tomograms were reconstructed in bin6 (14.34 A/pix). The reconstructed tomograms were denoised using cryoCARE[63] and these denoised tomograms were corrected for missing wedge using IsoNet[64]. The missing wedge-corrected tomograms were analyzed manually for the presence of ER, endosomes/lysosomes, mitochondria, and ribosomes. Correlative images (Fluorescence/tomogram) were analyzed using the Fiji distribution of ImageJ (National Institutes of Health)[65]. To create the template for the ribosomal identification, the top 5 tomograms with the highest number of ribosomes were chosen. From these 5 tomograms, around 1100 ribosomes were manually picked for initial template and the particle positions were refined, aligned, and averaged using Relion4 3D Refine up to bin4 (pixel size = 9.56 A)[66]. Template matching was performed using pytom-match-pick[67] and the false positive matches were manually cleaned afterwards. Selected tomograms were further analyzed for fluorescence-structure correlation, segmentation and ribosome positioning. The missing wedge-corrected tomograms were automatically segmented using MemBrain v2. The segmentations were manually cleaned and the organelles of interest (lysosome, ER, mitochondria) were selected using a software tool developed by the Mattei team (available upon request). The segmentations of the organelles, in-bin2-Relion-refined coordinates and orientations, 22 A ribosomes were plotted in the tomogram using ArtiaX plug-in of ChimeraX[68,69].

Statistical analysis and quantification

Statistics and reproducibility. The presented data are expressed as mean ± SEM, unless otherwise stated. Graphical representation and statistical analysis were conducted using GraphPad Prism (version 9.1.0) for Windows (GraphPad Software, San Diego, California, USA, www.graphpad.com) or Microsoft Excel. To compare two conditions a two-sided (paired or unpaired) Student's *t* test was employed, while a one-way or two-way ANOVA with Tukey's or Šídák's multiple comparison tests was used for analysis of one or two variables, respectively, within multiple groups. All datasets derive from at least three independent experiments unless otherwise indicated. No statistical methods were used to predetermine sample sizes, and no data were excluded from the analyses. For each dataset, the sample size (*n*), the number of independent biological repeats/experiments, and exact *p*-values are stated in the corresponding figures or figure legends.

Quantification of immunoblot images. Immunoblot images were obtained using the Invitrogen iBright FL1000 Imaging System (Thermo Fisher Scientific). Densitometric quantification of protein bands was performed using standard tools in the Fiji distribution of ImageJ (National Institutes of Health)[65]. Briefly, rectangular regions of interest (ROIs) of identical dimensions were drawn around each band of interest within a blot. The integrated density for each target protein band was measured and normalized to the corresponding loading control band within the same lane.

Quantification of microscopy images. Microscopy data quantification was carried out using Fiji/ImageJ[65]. Researchers were blinded to the experimental conditions. Images are displayed in grayscale (with signal inversion) when assessing the appearance of specific structures (SunTag clusters, PLA dots) involving a single channel. However, when the analysis involved colocalization between different signals/channels, the images were presented in pseudocolor.

Analysis of PINK1-SunTag clusters (number, intensity, area and colocalization with organelles). SunTag clusters are defined as discrete, local accumulations of scFv-GFP/mRaspberry/mScarlet signal rising above background. The morphology, size and distribution of these clusters depend on the specific reporter construct expressed (e.g., punctate cytosolic/mitochondrial dots for PINK1-SunTag$_{cyto}$, elongated structures co-aligning with mitochondrial membranes for PINK1-SunTag$_{mito}$), rather than intrinsic properties of the scFv-GFP/mRaspberry/mScarlet itself. In the absence of a SunTag-tagged reporter, scFv- GFP/mRaspberry/mScarlet remains diffusely distributed throughout the cytoplasm without forming clusters.

Quantification of cluster number. For the analysis of the number of clusters, the function 'find edges' in Fiji/ImageJ was used to define the contour of the clusters on z-projection images of the somas. Identified structures were then automatically counted and plotted per neuron.

Quantification of cluster intensity. To measure the mean fluorescent intensity of SunTag clusters, maximum z-projections were generated across a square-shaped region including the entire cell body. A duplicate image of the scFv-GFP (SunTag signal) channel was generated and thresholded. The "Analyze Particle" plugin (size threshold set from 5 pixels to infinity) was then applied to automatically detect discrete clusters and convert them into ROIs. These cluster ROIs were projected back onto the original, non-thresholded GFP image (SunTag signal) to extract the raw mean gray value (fluorescence intensity) for each cluster, which were averaged to yield an initial mean cluster intensity for that cell. To eliminate the contribution of diffuse cytosolic scFv-GFP, a representative background square ROI was drawn within a region of the soma devoid of SunTag clusters, and its mean gray value was subtracted from the overall mean cluster intensity of the neuron. Thus, a single background-subtracted mean cluster intensity value was obtained for each neuron.

Quantification of cluster area. To quantify cluster area, maximum z-projections encompassing the entire cell body were used. The ROIs defined by particle analyzer of the thresholded scFv-GFP (SunTag signal) channel (size threshold set from 5 pixels to infinity) were used to extract the area of each individual SunTag cluster. These area

values were averaged across all identified clusters within a given cell. Thus, a single mean cluster area value was obtained for each neuron.

Quantification of cluster colocalization with organelles. To determine colocalization between SunTag clusters and organellar markers (mitochondria, endolysosomes), analysis was performed on full z-stack images including the entire cell body without maximum z-projection using the JaCoP plugin[70] in Fiji/ImageJ. Colocalization was quantified using the Manders' colocalization coefficient. Manders' coefficients provide a pixel-overlap-based measure, evaluating the fraction of fluorescence signal above threshold in one channel that spatially overlaps with fluorescence signal in the second channel, independent of signal intensities between channels. Manders' values range from 0 (complete spatial exclusion) to 1 (complete spatial overlap). Where indicated, to verify that a high Manders' coefficient represented true biological colocalization rather than incidental overlap caused by high organelle density, a spatial specificity control (90° rotation of one channel) was performed. A $10 \times 10\,\mu m$ square region within the cell body (excluding the nucleus) was defined based on the organelle channel, and the Manders' colocalization coefficient was calculated before and after rotating the scFv-GFP (SunTag signal) channel by 90°. A significant loss of signal overlap upon rotation confirmed specificity.

All Manders' coefficient values, mean gray values (intensities) and area values were exported to Excel and plotted using GraphPad Prism.

Analysis of *Pink1* mRNA localization. To quantify *Pink1* mRNA localization relative to endolysosomes, full z-stack images including the entire cell body without maximum z-projection were analyzed using the JaCoP plugin in Fiji/ImageJ as described before[19,20,71] and as described for the PINK1-SunTag cluster analysis above. The colocalization between the *Pink1* mRNA reporter signal (Venus channel) and the endolysosomal channel was quantified using Manders' colocalization coefficient. The resulting Manders' colocalization coefficients were exported to Excel and plotted using GraphPad Prism.

Analysis of optineurin and phospho-ubiquitin stainings. To determine the accumulation of optineurin and phospho-ubiquitin at mitochondria, analysis was performed along intact neurites identified by βIII-tubulin immunostaining. Maximum z-projections were generated, and neurite segments were straightened using the 'straighten' feature in Fiji/ImageJ with a 20- or 50-pixel width margin. Colocalization between the optineurin or phospho-ubiquitin signal and the mitochondrial marker along the straightened neurite was quantified using Manders' colocalization coefficient via the JaCoP plugin in Fiji/ImageJ as described before[19,20]. The resulting Manders' colocalization coefficients were exported to Excel and plotted using GraphPad Prism.

Analysis of Parkin recruitment to mitochondria. To determine Parkin positive mitochondria as described previously[19,20], plots of fluorescence intensity versus the position along axons were generated using the 'Plot Profile' function of Fiji/ImageJ. A mitochondrion was considered Parkin positive when the intensity of the respective YFP-Parkin peak was at least twice as high as the baseline intensity level.

Reporting summary

Further information on research design is available in the Nature Portfolio Reporting Summary linked to this article.

Data availability

All data supporting the findings of this study are available within the article and Supplementary Information. Source data are provided with this paper. Microscopy data, constructs and unique reagents reported in this paper will be shared by the lead contact Angelika B. Harbauer (angelika.harbauer@tum.de) upon reasonable request. Source data are provided with this paper.

Code availability

A custom software tool for organelle annotation was used and is available under https://github.com/embl-ic/mattei-research/tree/main/harbauer_paper.

References

1. Murali Mahadevan, H., Hashemiaghdam, A., Ashrafi, G. & Harbauer, A. B. Mitochondria in neuronal health: from energy metabolism to Parkinson's disease. *Adv. Biol.* **5**, 2100663 (2021).
2. Valente, E. M. et al. PINK1 mutations are associated with sporadic early-onset parkinsonism. *Ann. Neurol.* **56**, 336–341 (2004).
3. Sekine, S. et al. Reciprocal roles of Tom7 and OMA1 during mitochondrial import and activation of PINK1. *Mol. Cell* **73**, 1028–1043.e5 (2019).
4. Jin, S. M. et al. Mitochondrial membrane potential regulates PINK1 import and proteolytic destabilization by PARL. *J. Cell Biol.* **191**, 933–942 (2010).
5. Greene, A. W. et al. Mitochondrial processing peptidase regulates PINK1 processing, import and Parkin recruitment. *EMBO Rep.* **13**, 378–385 (2012).
6. Yamano, K. & Youle, R. J. PINK1 is degraded through the N-end rule pathway. *Autophagy* **9**, 1758–1769 (2013).
7. Yoo, L. & Chung, K. C. The ubiquitin E3 ligase CHIP promotes proteasomal degradation of the serine/threonine protein kinase PINK1 during staurosporine-induced cell death. *J. Biol. Chem.* **293**, 1286–1297 (2018).
8. Narendra, D. P. et al. PINK1 is selectively stabilized on impaired mitochondria to activate parkin. *PLoS Biol.* **8**, e1000298 (2010).
9. Lazarou, M., Jin, S. M., Kane, L. A. & Youle, R. J. Role of PINK1 binding to the TOM complex and alternate intracellular membranes in recruitment and activation of the E3 ligase Parkin. *Dev. Cell* **22**, 320–333 (2012).
10. Okatsu, K. et al. PINK1 autophosphorylation upon membrane potential dissipation is essential for Parkin recruitment to damaged mitochondria. *Nat. Commun.* **3**, 1016 (2012).
11. Kane, L. A. et al. PINK1 phosphorylates ubiquitin to activate Parkin E3 ubiquitin ligase activity. *J. Cell Biol.* **205**, 143–153 (2014).
12. Kazlauskaite, A. et al. Parkin is activated by PINK1-dependent phosphorylation of ubiquitin at Ser65. *Biochem. J.* **460**, 127–141 (2014).
13. Koyano, F. et al. Ubiquitin is phosphorylated by PINK1 to activate parkin. *Nature* **510**, 162–166 (2014).
14. Yamano, K., Matsuda, N. & Tanaka, K. The ubiquitin signal and autophagy: an orchestrated dance leading to mitochondrial degradation. *EMBO Rep.* **17**, 300–316 (2016).
15. Shiba-Fukushima, K. et al. PINK1-mediated phosphorylation of the Parkin ubiquitin-like domain primes mitochondrial translocation of Parkin and regulates mitophagy. *Sci. Rep.* **2**, 1002 (2012).
16. Ordureau, A. et al. Quantitative proteomics reveal a feedforward mechanism for mitochondrial PARKIN translocation and ubiquitin chain synthesis. *Mol. Cell* **56**, 360–375 (2014).
17. Wong, Y. C. & Holzbaur, E. L. F. Optineurin is an autophagy receptor for damaged mitochondria in parkin-mediated mitophagy that is disrupted by an ALS-linked mutation. *Proc. Natl. Acad. Sci.* USA **111**, E4439-48 (2014).
18. Lazarou, M. et al. The ubiquitin kinase PINK1 recruits autophagy receptors to induce mitophagy. *Nature* **524**, 309–314 (2015).
19. Harbauer, A. B. et al. Neuronal mitochondria transport Pink1 mRNA via synaptojanin 2 to support local mitophagy. *Neuron* **110**, 1516–1531.e9 (2022).

20. Hees, J. T. et al. Insulin signalling regulates Pink1 mRNA localization via modulation of AMPK activity to support PINK1 function in neurons. *Nat. Metab.* **6**, 514–530 (2024).
21. Sekine, S. & Youle, R. J. PINK1 import regulation; a fine system to convey mitochondrial stress to the cytosol. *BMC Biol.* **16**, 2 (2018).
22. Luo, J. et al. Proximity-specific ribosome profiling reveals the logic of localized mitochondrial translation. *Cell* **188**, 5589–5604.e17 (2025).
23. Zhu, Z. et al. Principles of cotranslational mitochondrial protein import. *Cell* **188**, 5605–5617.e14 (2025).
24. Hansen, K. G. et al. An ER surface retrieval pathway safeguards the import of mitochondrial membrane proteins in yeast. *Science* **361**, 1118–1122 (2018).
25. Tanenbaum, M. E., Gilbert, L. A., Qi, L. S., Weissman, J. S. & Vale, R. D. A Protein-tagging system for signal amplification in gene expression and fluorescence imaging. *Cell* **159**, 635–646 (2014).
26. O'Callaghan, B. et al. Glucose concentration of neuronal media formulations influences PINK1-dependent mitophagy in human iNeurons. *Autophagy Rep.* **5**, 2685472 (2026).
27. Schofield, C. J. & Ratcliffe, P. J. Oxygen sensing by HIF hydroxylases. *Nat. Rev. Mol. Cell Biol.* **5**, 343–354 (2004).
28. Chan, D. A., Sutphin, P. D., Yen, S.-E. & Giaccia, A. J. Coordinate regulation of the oxygen-dependent degradation domains of hypoxia-inducible factor 1 alpha. *Mol. Cell. Biol.* **25**, 6415–6426 (2005).
29. Wu, B., Chen, J. & Singer, R. H. Background free imaging of single mRNAs in live cells using split fluorescent proteins. *Sci. Rep.* **4**, 3615 (2014).
30. Alam, M. S. Proximity Ligation Assay (PLA). *Curr. Protoc. Immunol.* **123**, e58 (2018).
31. Tom Dieck, S. et al. Direct visualization of newly synthesized target proteins in situ. *Nat. Methods* **12**, 411–414 (2015).
32. Cioni, J.-M. et al. Late endosomes act as mRNA translation platforms and sustain mitochondria in axons. *Cell* **176**, 56–72.e15 (2019).
33. Hu, Y.-B., Dammer, E. B., Ren, R.-J. & Wang, G. The endosomal-lysosomal system: from acidification and cargo sorting to neurodegeneration. *Transl. Neurodegener.* **4**, 18 (2015).
34. Jan, C. H., Williams, C. C. & Weissman, J. S. Principles of ER cotranslational translocation revealed by proximity-specific ribosome profiling. *Science* **346**, 1257521 (2014).
35. Hung, V. et al. Proteomic mapping of cytosol-facing outer mitochondrial and ER membranes in living human cells by proximity biotinylation. *eLife* **6**, e24463 (2017).
36. Anastasia, I. et al. Mitochondria-rough-ER contacts in the liver regulate systemic lipid homeostasis. *Cell Rep.* **34**, 108873 (2021).
37. Koch, C. et al. The ER-SURF pathway uses ER-mitochondria contact sites for protein targeting to mitochondria. *EMBO Rep.* **25**, 2071–2096 (2024).
38. Rai, P. et al. IRGM1 links mitochondrial quality control to autoimmunity. *Nat. Immunol.* **22**, 312–321 (2021).
39. Smith, C. & D'Mello, S. R. Cell and context-dependent effects of the heat shock protein DNAJB6 on neuronal survival. *Mol. Neurobiol.* **53**, 5628–5639 (2016).
40. Liao, Y.-C. et al. RNA granules hitchhike on lysosomes for long-distance transport, using annexin A11 as a molecular tether. *Cell* **179**, 147–164.e20 (2019).
41. Schuhmacher, J. S. et al. The Rab5 effector FERRY links early endosomes with mRNA localization. *Mol. Cell* **83**, 1839–1855.e13 (2023).
42. De Pace, R. et al. Messenger RNA transport on lysosomal vesicles maintains axonal mitochondrial homeostasis and prevents axonal degeneration. *Nat. Neurosci.* **27**, 1087–1102 (2024).
43. Holt, C. E., Martin, K. C. & Schuman, E. M. Local translation in neurons: visualization and function. *Nat. Struct. Mol. Biol.* **26**, 557–566 (2019).
44. Koppers, M. et al. Axonal endoplasmic reticulum tubules control local translation via P180/RRBP1-mediated ribosome interactions. *Dev. Cell* **59**, 2053–2068.e9 (2024).
45. Martin-Solana, E. et al. Ribosome-associated vesicles promote activity-dependent local translation in neurons. Preprint at https://doi.org/10.1101/2024.06.07.598007 (2024).
46. Eldeeb, M. A. et al. Tom20 gates PINK1 activity and mediates its tethering of the TOM and TIM23 translocases upon mitochondrial stress. *Proc. Natl. Acad. Sci. USA* **121**, e2313540121 (2024).
47. Callegari, S. et al. Structure of human PINK1 at a mitochondrial TOM-VDAC array. *Science* **388**, 303–310 (2025).
48. Guardia-Laguarta, C. et al. PINK1 content in mitochondria is regulated by ER-associated degradation. *J. Neurosci.* **39**, 7074–7085 (2019).
49. Kim, N. C. et al. VCP is essential for mitochondrial quality control by PINK1/Parkin and this function is impaired by VCP mutations. *Neuron* **78**, 65–80 (2013).
50. Choi, H. et al. Secretome translation shaped by lysosomes and lunapark-marked ER junctions. *Nature* **649**, 227–236 (2026).
51. Rose, J. M., Novoselov, S. S., Robinson, P. A. & Cheetham, M. E. Molecular chaperone-mediated rescue of mitophagy by a Parkin RING1 domain mutant. *Hum. Mol. Genet.* **20**, 16–27 (2011).
52. Arkan, S., Ljungberg, M., Kirik, D. & Hansen, C. DNAJB6 suppresses alpha-synuclein induced pathology in an animal model of Parkinson's disease. *Neurobiol. Dis.* **158**, 105477 (2021).
53. Rodríguez-González, C., Lin, S., Arkan, S. & Hansen, C. Co-chaperones DNAJA1 and DNAJB6 are critical for regulation of polyglutamine aggregation. *Sci. Rep.* **10**, 8130 (2020).
54. Durrenberger, P. F. et al. DnaJB6 is present in the core of Lewy bodies and is highly up-regulated in parkinsonian astrocytes. *J. Neurosci. Res.* **87**, 238–245 (2009).
55. Zhang, Y. et al. Rapid single-step induction of functional neurons from human pluripotent stem cells. *Neuron* **78**, 785–798 (2013).
56. van den Ent, F. & Löwe, J. RF cloning: a restriction-free method for inserting target genes into plasmids. *J. Biochem. Biophys. Methods* **67**, 67–74 (2006).
57. Johnston, A. J. et al. Insertion and assembly of human tom7 into the preprotein translocase complex of the outer mitochondrial membrane. *J. Biol. Chem.* **277**, 42197–42204 (2002).
58. Kislinger, G. et al. ATUM-FIB microscopy for targeting and multi-scale imaging of rare events in mouse cortex. *STAR Protoc.* **1**, 100232 (2020).
59. Kislinger, G. et al. Neurons on tape: automated tape collecting ultramicrotomy-mediated volume EM for targeting neuropathology. *Methods Cell Biol.* **177**, 125–170 (2023).
60. Zivanov, J. et al. A Bayesian approach to single-particle electron cryo-tomography in RELION-4.0. *eLife* **11**, e83724 (2022).
61. Tegunov, D., Xue, L., Dienemann, C., Cramer, P. & Mahamid, J. Multi-particle cryo-EM refinement with M visualizes ribosome-antibiotic complex at 3.5 Å in cells. *Nat. Methods* **18**, 186–193 (2021).
62. Zheng, S. et al. AreTomo: An integrated software package for automated marker-free, motion-corrected cryo-electron tomographic alignment and reconstruction. *J. Struct. Biol. X* **6**, 100068 (2022).
63. Buchholz, T.-O., Jordan, M., Pigino, G. & Jug, F. Cryo-CARE: content-aware image restoration for cryo-transmission electron microscopy data. in *2019 IEEE 16th International Symposium on Biomedical Imaging (ISBI 2019)*, 502–506 (IEEE, 2019). https://doi.org/10.1109/ISBI.2019.8759519.
64. Liu, Y.-T. et al. Isotropic reconstruction for electron tomography with deep learning. *Nat. Commun.* **13**, 6482 (2022).

65. Schindelin, J. et al. Fiji: an open-source platform for biological-image analysis. *Nat. Methods* **9**, 676–682 (2012).
66. Kimanius, D., Dong, L., Sharov, G., Nakane, T. & Scheres, S. H. W. New tools for automated cryo-EM single-particle analysis in RELION-4.0. *Biochem. J.* **478**, 4169–4185 (2021).
67. Chaillet, M. L., Roet, S., Veltkamp, R. C. & Förster, F. pytom-match-pick: a tophat-transform constraint for automated classification in template matching. *J. Struct. Biol. X* **11**, 100125 (2025).
68. Ermel, U. H., Arghittu, S. M. & Frangakis, A. S. ArtiaX: an electron tomography toolbox for the interactive handling of sub-tomograms in UCSF ChimeraX. *Protein Sci. Publ. Protein Soc.* **31**, e4472 (2022).
69. Meng, E. C. et al. UCSF ChimeraX: tools for structure building and analysis. *Protein Sci. Publ. Protein Soc.* **32**, e4792 (2023).
70. Bolte, S. & Cordelières, F. P. A guided tour into subcellular colocalization analysis in light microscopy. *J. Microsc.* **224**, 213–232 (2006).
71. Graber, T. E. et al. Reactivation of stalled polyribosomes in synaptic plasticity. *Proc. Natl. Acad. Sci. USA* **110**, 16205–16210 (2013).

Acknowledgements

We thank C. Weiß, M. Martins, C. Niemann, and G. Kislinger for technical support and all the members of the Harbauer laboratory for their support and many fruitful discussions. We are grateful to the Imaging facilities of the MPIs for Biological Intelligence (RRID:SCR_026797) and Biochemistry (RRID:SCR_025739), for assistance with live cell imaging. We are also extremely grateful for the assistance of D. Bollschweiler and T. Schäfer from the CryoEM facility at the MPI for Biochemistry (RRID:SCR_025744) for their help with sample preparation and analysis. We are grateful for the assistance of Z. Yang and acknowledge the access and services provided by the Imaging Centre at the European Molecular Biology Laboratory (EMBL-IC), generously supported by the Boehringer Ingelheim Foundation. We thank the EMBL central IT services and Thomas Hoffmann for computational support.

Author contributions

A.B.H. conceived the project and wrote the manuscript together with J.T.H. and I.S., with additional input from T.M., M.S. and A.S. J.T.H. and I.S. designed and conducted most of the experiments. A.S. was responsible for the BirA assays. M.S. and T.M. were responsible for CLEM imaging. I.S., S.B. and S.M. were responsible for the Cryo-ET imaging. J.L. was responsible for the primary mouse neuron culture and human iPSC culture as well as neuronal differentiation. All authors read and approved the manuscript.

Funding

Work in ABH's lab is supported by the Max Planck Society, DFG (DFG, TRR353 – ID 471011418, SPP ID 541742535), the European Union (ERC StG Project 101077138 — MitoPIP) and Germany's Excellence Strategy within the framework of the Munich Cluster for Systems Neurology (EXC 2145 SyNergy – ID 390857198) and the Schram foundation (T0287/46550/2025). Work in TM's lab is supported by the DFG (Mi 694/8-1), FOR Immunostroke (Mi 694/9-1/2 – ID 428663564). TM and MS received funds via TRR 274/1 Projects C02, Z01, respectively (ID 408885537). TM is a member of and supported by the German Center for Neurodegenerative Diseases (DZNE). High-resolution microscopy was supported via a DFG instrumentation grant (INST95/1755-1 FUGG, ID 518284373). TM and MS are supported by a Chan Zuckerberg Initiative (CZI) grant for Creating Community & Building Capacity. ABH, MS and TM are supported by Germany's Excellence Strategy within the framework of the Munich Cluster for Systems Neurology (EXC 2145 SyNergy – ID 390857198). Work in SM's lab was funded by the DFG – SPP2453 project number 541626282. This work benefited from access to the EMBL Heidelberg, an Instruct-ERIC centre. Financial support was provided by Instruct-ERIC (PID 36994). Open Access funding enabled and organized by Projekt DEAL.

Competing interests

The authors declare no competing interests.

Additional information

Supplementary information The online version contains supplementary material available at https://doi.org/10.1038/s41467-026-79754-5.

Correspondence and requests for materials should be addressed to Angelika B. Harbauer.

Peer review information *Nature Communications* thanks Suzan Ruijtenberg who co-reviewed with Loes Stellerand the other anonymous reviewer(s) for their contribution to the peer review of this work. A peer review file is available.

Reprints and permissions information is available at http://www.nature.com/reprints

Publisher's note Springer Nature remains neutral with regard to jurisdictional claims in published maps and institutional affiliations.

Open Access This article is licensed under a Creative Commons Attribution 4.0 International License, which permits use, sharing, adaptation, distribution and reproduction in any medium or format, as long as you give appropriate credit to the original author(s) and the source, provide a link to the Creative Commons licence, and indicate if changes were made. The images or other third party material in this article are included in the article's Creative Commons licence, unless indicated otherwise in a credit line to the material. If material is not included in the article's Creative Commons licence and your intended use is not permitted by statutory regulation or exceeds the permitted use, you will need to obtain permission directly from the copyright holder. To view a copy of this licence, visit http://creativecommons.org/licenses/by/4.0/.

© The Author(s) 2026